Progressive drought transcriptomics and co-expression framework in eggplant (*Solanum melongena* L.)

Matteo Martina[1+], Cristina Morabito[1+], Andrea Moglia[1], Anna Maria Milani[1], Lorenzo Barchi[1], Alberto Acquadro[1], Cinzia Comino[1*], Francesca Secchi[1*], Ezio Portis1

1. Dipartimento di Scienze Agrarie, Forestali e Alimentari (DISAFA), Università degli Studi di Torino, Largo P. Braccini 2, Grugliasco (TO)

[+] These authors contributed equally to this work.
* cinzia.comino@unito.it; francesca.secchi@unito.it

Abstract

Drought is a major constraint for eggplant productivity in Mediterranean and semi-arid environments, yet stage-specific molecular features that distinguish tolerant and sensitive genotypes under progressive water deficit remain limited. Here, we profiled drought responses in two contrasting eggplant (Solanum melongena L.) genotypes from the G2P-SOL core collection, integrating physiology and transcriptomics to resolve genotype-dependent programs at moderate and severe stress. Physiological measurements confirmed divergent drought performance, with the tolerant genotype 'Berenjena de rabo largo' (GPE020510) maintaining water status and stomatal function longer than the sensitive genotype 'Qianzi' (GPE008940). RNA-seq revealed strong transcriptional reprogramming in both genotypes, but with distinct timing and functional priorities across stress transitions. At moderate stress, tolerance was associated with early ABA-centred regulatory control and dehydration protection (including ABI5, TAS14 and LEA/dehydrin-related loci), coupled to transport and redox homeostasis and repression of growth-associated outputs. In contrast, the sensitive genotype showed prominent early regulatory and RNA/protein-turnover signatures alongside weaker representation of cuticle/barrier and chloroplast/light-management functions. Under severe stress, the sensitive genotype shifted toward a broad high-maintenance state enriched in remodeling, detoxification and transporter activity, whereas the tolerant genotype displayed a more targeted adjustment featuring plastid photoprotection, proteostasis and selective metabolic reconfiguration. Co-expression network analysis supported this stage-resolved model by identifying modules and hub genes with contrasting temporal trajectories between genotypes, linking earlier coordinated regulatory/membrane-trafficking and plastid/redox tuning to drought tolerance. Overall, these results indicate that eggplant drought resilience is associated with genotype-specific coordination and timing of protective programs superimposed on a shared basal stress response, and they provide prioritized candidate pathways and genes for functional validation and breeding.

Introduction

Drought is a dominant constraint for crop productivity and quality (Paladini et al., 2025; Seleiman et al., 2021), and its effects are expected to intensify as climate variability increases the frequency of irregular rainfall and heat–dry spells (Abbass et al., 2022; Araus and Kefauver, 2018; Dai, 2013; Haile et al., 2024). For fleshy-fruited vegetable crops, water deficit is particularly impactful because yield formation relies on sustained carbon assimilation, source–sink coordination, and maintenance of cellular homeostasis during prolonged developmental windows (Ahluwalia et al., 2021; Fahad et al., 2017; Seleiman et al., 2021; Yıldız and Akı, 2025). In Solanaceae, drought commonly triggers a cascade of interconnected processes such as stomatal limitation and altered carbon allocation, membrane and cell-wall remodeling, shifts in redox balance and detox capacity, and a progressive reconfiguration of growth programs that together determine whether plants remain functional under moderate stress or transition to severe-stress states that can be associated with irreversible performance losses (Blanchard-Gros et al., 2022; Emami Bistgani et al., 2024; Maioli et al., 2024; Martina et al., 2024; Ojeilua et al., 2025; Pang et al., 2024; Saptiningsih et al., 2023; Wadood et al., 2024; Yıldız and Akı, 2025). As drought typically develops along a continuum rather than as a binary event, a key conceptual challenge is to understand how plants move from moderate to severe stress and which molecular features distinguish these stages.

Eggplant (*Solanum melongena* L.) is a major vegetable crop in Mediterranean and semi-arid regions, where tightening irrigation and more frequent heat–drought episodes increasingly penalize yield and quality (Gaccione et al., 2023; Sękara et al., 2016; Toppino et al., 2022; Villanueva et al., 2026). Yet, compared with model species, drought-response frameworks in eggplant are still relatively fragmented, and markers that robustly separate tolerant from susceptible genotypes remain limited. Recent studies nonetheless provide clear mechanistic and genomic entry points. Functional evidence shows that the bHLH regulator SmMYC2 can enhance drought resilience by promoting secondary cell wall thickening through SmNST1-linked regulation, supporting cell-wall reinforcement as a relevant tolerance output(Li et al., 2025). Severity-aware transcriptomics further indicate that drought responses depend strongly on stress intensity and developmental context: RNA-seq across two PEG levels and two exposure times showed that the wild relative (*S. dasyphyllum*) is more water-deficit tolerant than cultivated eggplant and deploys broader drought TF repertoires (AP2/ERF, DREB, bZIP, WRKY, bHLH), with ABA signaling as a central axis and additional involvement of phenylpropanoid/flavonoid and carotenoid metabolism, chlorophyll metabolism, and photosynthesis-related pathways under both moderate and severe regimes (Villanueva et al., 2023). Physiological studies across wild relatives and interspecific hybrids similarly report strong drought impacts on growth and tissue water content together with increases in biochemical stress markers such as proline and MDA, underscoring polygenic control and diverse stress strategies (González-Orenga et al., 2023). However, single time points or single severity levels can confound early acclimation with late damage-control programs. Disentangling these phases requires designs that explicitly compare moderate and severe drought in contrasting genotypes and interpret expression as stage-specific programs rather than static lists of "drought genes".

Here, we address this gap by contrasting two eggplant genotypes with divergent drought performance across progressive stress stages, focusing on transitions that capture (i) the onset of moderate drought (T0 to WS-M) and (ii) drought escalation from moderate to severe stress (WS-M to WS-S). We integrate three complementary transcriptome layers-differential expression, GSEA-based functional directionality, and WGCNA module/hub structure to ask whether tolerance is associated with early engagement of protective and homeostasis-buffering programs, and whether susceptibility is associated with early regulatory rewiring that is not accompanied by coherent deployment of barrier- and plastid-

support functions. We further test, at the level of co-expression architecture, whether the WS-M to WS-S transition is dominated by broad severity-associated "maintenance-mode" programs in the susceptible genotype, versus more targeted plastid/light-management and redox-associated programs in the tolerant genotype.

By building a staged, genotype-aware framework, this study aims to move beyond single-gene narratives and instead provide a systems description of drought-response trajectories in eggplant. The resulting interpretation yields (i) stage-resolved candidate processes that can be linked to tolerance versus susceptibility as hypotheses, (ii) prioritized candidate genes and module hubs that anchor these hypotheses, and (iii) a template for future targeted experimentation to test whether the inferred programs translate into measurable protective outputs.

Materials and Methods

Plant material and experimental design

Two eggplant (*Solanum melongena* L.) genotypes from the G2P-SOL core collection (http://www.g2p-sol.eu/) were selected based on their contrasting responses to drought stress previously characterized within the G2P-SOL framework. The drought-tolerant genotype '*Berenjena de rabo largo*' (GPE020510), originating from Spain, and the drought-sensitive genotype Qianzi (GPE008940), originating from China, were used in this study. Seeds were germinated in a growth chamber under controlled conditions (25/18 °C day/night, 16 h light/8 h dark photoperiod, 60–70% relative humidity). At the four-leaf stage, seedlings were transplanted into 1 L pots filled with a standardized peat/perlite substrate (3:1, v/v) and transferred to a greenhouse for further growth. Thirty-eight plants were irrigated daily to pot capacity until the onset of drought treatment. At the 12-leaf stage, 18 plants (9 per genotype) were maintained under well-watered conditions (controls), while the remaining 20 (10 for genotype) were subjected to a progressive reduction in water availability (stressed) starting on day 0. Water stress was imposed by restoring 80% of the water lost on the previous day, with pot weight measured every morning. Drought stress was imposed gradually and monitored through plant water status, allowing the definition of two physiological sampling points: moderate water stress (WS-M), corresponding to a leaf water potential of approximately −1.0 MPa, and severe water stress (WS-S), corresponding to a leaf water potential of approximately −2.0 MPa. Plant sampling (n=3 for controls, n=5 for stressed) for physiological and transcriptomic analyses was performed at these defined physiological stages.

Physiological measures

Stem water potential (Ψ) was measured during drought progression. Measurements were performed at midday on fully expanded, non-transpiring leaves using a Scholander-type pressure chamber, following standard procedures (Morabito et al., 2022). For each genotype and condition, three individual plants were selected and one leaf per plant was measured. Stem water potential data were used to quantify the severity of water stress and to compare the physiological responses of the two eggplant genotypes under control and drought conditions.

Stomatal conductance was measured on fully expanded leaves using a portable gas exchange system (LI-6800, LI-COR Biosciences). CO_2 concentration entering the cuvette was set to 400 µmol CO_2 mol^{-1} air, and relative humidity was set to follow environmental conditions. Measurements were conducted

on all plants (one leaf per plant) between 10.00 a.m. and 12.00 p.m. under ambient environmental conditions to minimize diurnal variation.

RNA extraction and sequencing

For transcriptome profiling, fully expanded leaves were collected at each sampling point from control and stressed plants of the two eggplant genotypes. Sampling was carried out on the same plants and at the same time point used for leaf water potential measurements. For each genotype and treatment, three biological replicates were collected, each consisting of a pooled leaves sample from an individual plant, which was immediately frozen in liquid nitrogen and stored at −80°C until processing. Total RNA was extracted from approximately 100 mg of powdered leaf tissue using a column-based plant RNA purification kit (Spectrum™ Plant Total RNA Kit, Sigma-Aldrich), followed by DNase treatment to remove residual genomic DNA. RNA concentration and purity were assessed spectrophotometrically, and RNA integrity was verified by agarose gel electrophoresis and capillary electrophoresis. Stranded mRNA libraries were prepared from poly(A)-enriched RNA according to standard Illumina protocols and sequenced as paired-end reads (2 × 150 bp) on an Illumina NovaSeq X Plus at Novogene Europe (Cambridge,UK) and Igatech (Udine, IT).

Read processing, transcript quantification and differential expression analysis

Raw sequencing reads were quality filtered and adapter-trimmed using fastp. Cleaned reads were pseudo-aligned to the *Solanum melongena* reference transcriptome (SMEL v5, '67/3' line; Gaccione et al., 2025) using Salmon in quasi-mapping mode with default parameters. Transcript abundances were quantified as counts and Transcripts Per Million (TPM), and gene-level count matrices were imported into R (Patro et al., 2017) using the tximport package (Soneson et al., 2015). Differential expression analysis was performed using DESeq2 (Love et al., 2014 - design *geno* + *condition* + *geno:condition*). The *geno* factor included two levels (GPE008940 and GPE020510), while *condition* represented the combination of time point (T0, WS-M and WS-S) and treatment (CTR and STR), with T0_CTR set as the reference level. Size-factor normalisation and dispersion estimation followed the standard DESeq2 workflow, and differential expression was assessed using Wald tests. Biologically relevant contrasts were defined to compare drought-stressed and control plants within each physiological stage, to evaluate transcriptional changes along drought progression, and to compare genotypes under identical experimental conditions. *p-values* were adjusted for multiple testing using the Benjamini–Hochberg false discovery rate (FDR - Benjamini and Hochberg, 1995). Genes with adjusted p-value < 0.05 were considered differentially expressed, and an additional threshold was applied for selected visualisations ($|\log_2 \text{fold change}| > 1$). For exploratory analyses, size-factor normalised counts were transformed using a $\log_2(\text{count} + 1)$ transformation and used for principal component analysis and heatmap generation with pheatmap (Kolde, 2010).

Gene set enrichment analysis (GSEA)

To investigate transcriptional changes at the pathway level, we performed Gene Set Enrichment Analysis (GSEA) using (Langfelder and Horvath, 2008) the *enrichplot* package (https://github.com/YuLab-SMU/enrichplot) in R. For each contrast of interest, all genes with non-missing $\log_2$ fold change were ranked according to the DESeq2 $\log_2$ fold change, with positive values indicating higher expression in the second level of the contrast. These ranked gene lists were used as input for the *gseGO* function, employing a dedicated *S. melongena* annotation package and SMEL5 gene identifiers as *keys*. Gene Ontology enrichment was carried out separately for the Biological

Process, Molecular Function and Cellular Component ontologies, using a minimum gene set size of 5 and a maximum of 500 genes. Significance of enrichment scores was assessed using a simple permutation scheme with 20,000 permutations, and *p-values* were adjusted for multiple testing using the Benjamini–Hochberg procedure. GO terms with an adjusted *p-value* $\leq$ 0.05 were considered significantly enriched. Enriched GO categories were visualized using the *enrichplot* package. Ridgeplots were generated to display, for each GO term, the distribution of ranked $\log_2$ fold changes of core enriched genes, with color scales encoding the adjusted p-value. In addition, mirrored dot plots were constructed to compare enrichment patterns between the two genotypes by jointly displaying, for each GO term, its presence in GPE022290 and/or GPE036890, and the size of the corresponding core gene sets. This representation allowed us to distinguish terms that were uniquely enriched in the sensitive line, uniquely enriched in the tolerant line, or shared between them.

Co-expression network analysis (WGCNA)

Weighted gene co-expression network analysis (WGCNA) was performed in R using the WGCNA package (Langfelder and Horvath, 2008) to identify modules of co-expressed genes showing coordinated transcriptional dynamics during drought progression in the two eggplant genotypes. Genes with low expression across samples were filtered prior to network construction. Normalized expression values derived from DESeq2 size-factor normalization were used as input and transformed to stabilize variance. To focus on transcriptional changes associated with stress progression rather than absolute baseline differences between genotypes, the analysis was conducted on expression changes relative to the baseline condition. For each genotype, expression values were centered by subtracting the genotype-specific mean expression at the T0_CTR condition, generating Δ-expression values that capture stage-dependent transcriptional variation across subsequent physiological stages. Pairwise gene co-expression similarity was quantified using Pearson correlations on Δ-expression values, and an adjacency matrix was constructed by applying a soft-thresholding power selected according to the scale-free topology criterion. The adjacency matrix was transformed into a topological overlap matrix (TOM), and genes were hierarchically clustered based on TOM dissimilarity. Co-expression modules were detected using dynamic tree cutting and subsequently merged based on eigengene similarity. Module eigengenes, defined as the first principal component of each module, were used to summarize module-level expression patterns across samples and to evaluate genotype-dependent trajectories along drought progression. Hub genes were identified within selected modules based on intramodular connectivity and module membership (kME) values.

Results

Physiological responses to water stress differ between genotypes

Under well-watered conditions (day 0), no significant differences were observed between the two genotypes (*i.e.* GPE008940 and GPE020510) for either stomatal conductance or stem water potential, indicating comparable physiological status at the onset of the experiment (Fig. 1). As water stress progressed, clear genotype-dependent differences emerged. Under water-limited conditions, stomatal conductance declined in both genotypes, but with markedly different dynamics. In GPE008940, stomatal conductance (gs) decreased sharply after 5 days of treatment, and at that time the stem water potential (ψstem) dropped to approximately -1MPa. Two days later, this genotype closed its stomata, and the ψstem reached values of about -2MPa. In contrast, GPE020510 did not show changes in either gs or ψstem after 5 days of stress imposition compared to their controls. These plants required more days to reach moderate and severe stress levels comparable to those experienced by the other genotype.

In GPE020510 plants, the stomatal conductance decreased after 7 days of stress, and the stomata were fully closed after 9 days, when stem water potential dropped to approximately -1.5 MPa.

Under well-watered conditions, both genotypes maintained stable stomatal conductance and stem water potential throughout the experiment, confirming that the observed differences were specifically associated with the water stress treatment rather than with developmental effects.

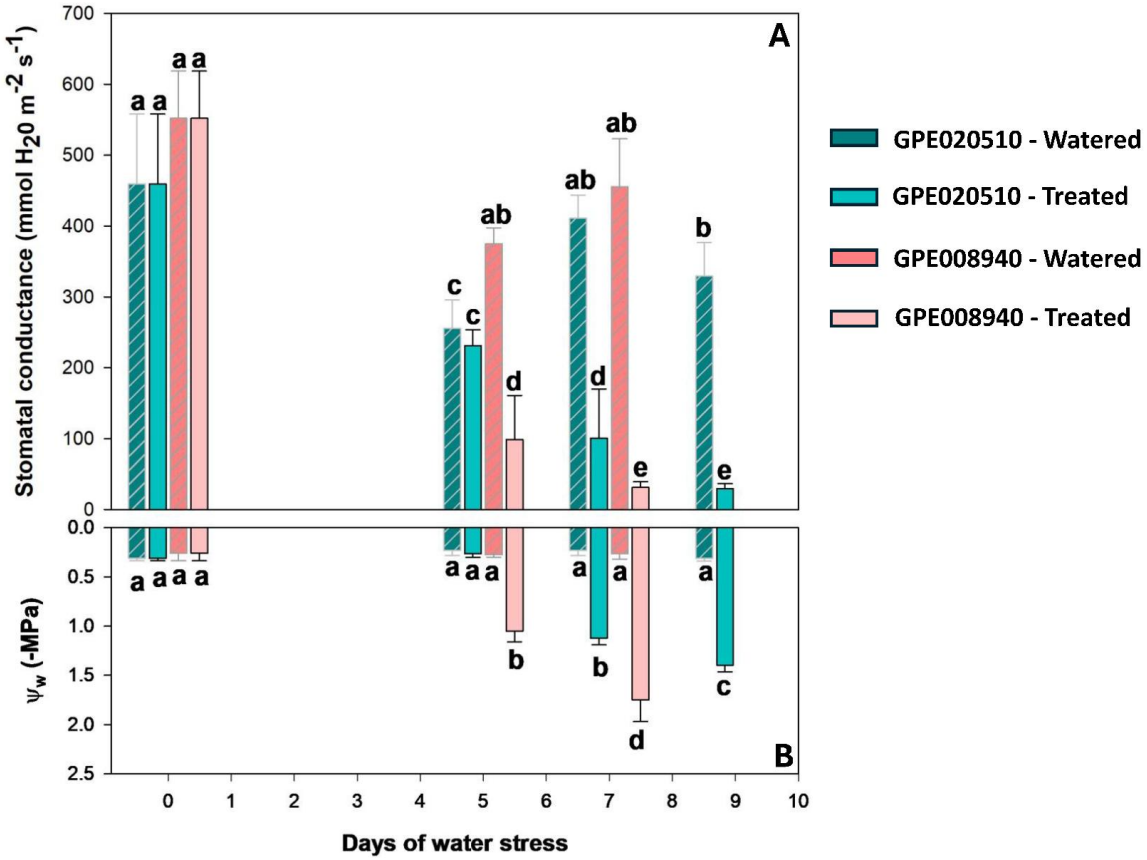

Figure 1. *(A) Stomatal conductance (gs; mmol H_2O m^{-2} s^{-1}) and (B) leaf water potential (Ψw; MPa) measured over the course of increasing days of water deficit. Bars represent the two genotypes (GPE020510 - green - and GPE008960 - red) under well-watered and water-stressed conditions (as indicated by the bar color/pattern in the legend). Data are shown as mean ± SE. Different letters above bars denote statistically significant differences among treatments/genotypes within each time point (post hoc test, P < 0.05).*

Transcriptomic variation under stress conditions

To assess genotype-dependent transcriptional divergence under drought stress, differential expression analyses were performed between GPE008940 and GPE020510 at two stress conditions, moderate (WS-M) and severe (WS-S). Principal component analysis revealed that, while drought stress accounted for the major source of transcriptomic variation, clear genotype-specific separation was evident within both stress conditions, with distinct patterns emerging at WS-M and WS-S (Figure 2A). Consistently, pairwise comparisons between genotypes identified thousands of differentially expressed genes under both stress levels (Figure 2B). As depicted by upset plot (Figure 2C), a core set of 1032 genes was shared by the two genotypes between WS-M and WS-S, together with stress-severity-specific gene subsets (81 in WS-M and 1043 in WS-S), suggesting that drought intensity modulates the transcriptional programs underlying genotype-dependent responses.

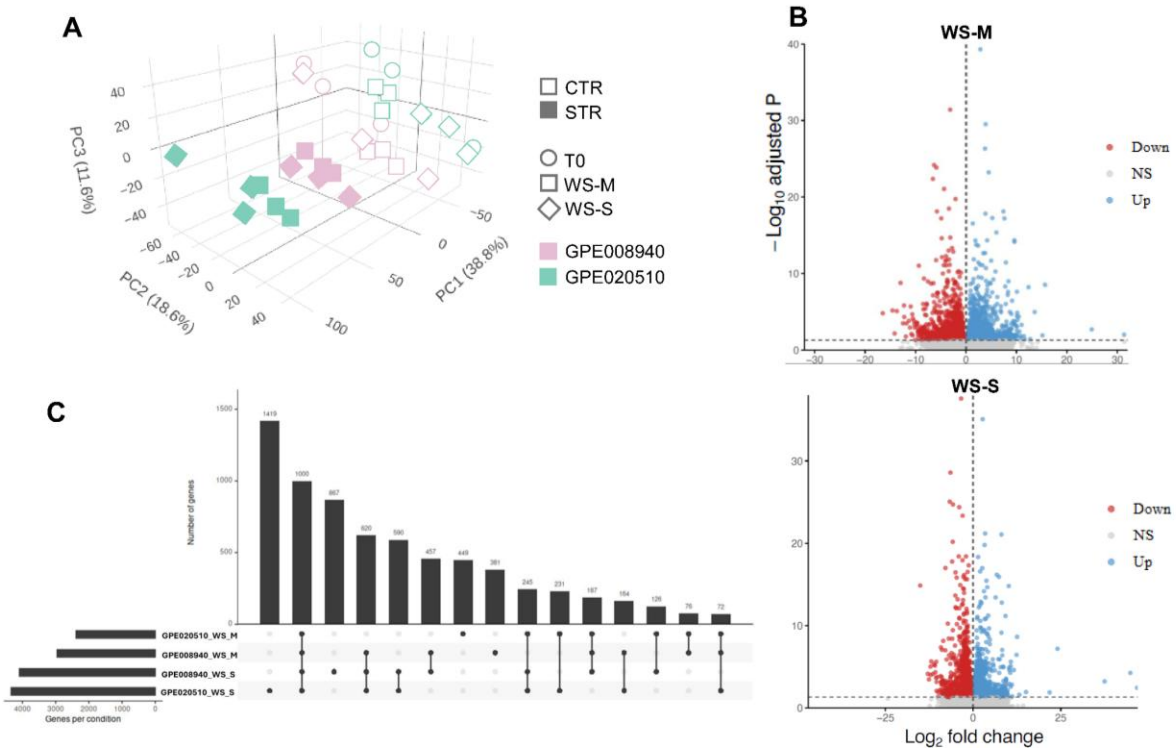

Figure 2. *(A) Three-dimensional PCA of variance-stabilized RNA-seq expression profiles showing clustering of samples by genotype and drought severity (moderate, WS-M; severe, WS-S), indicating progressive transcriptome reprogramming with stress intensification. Axes report the percentage of variance explained by each principal component. (B) Volcano plots of differential expression highlighting drought-responsive genes (FDR-adjusted P and log_2 fold-change thresholds as indicated by dashed lines), with upregulated genes in blue, downregulated genes in red, and non-significant genes in grey. (C) UpSet plot summarizing the size and overlap of drought-responsive gene sets across genotype × severity contrasts, illustrating shared and genotype-/stage-specific transcriptional programs.*

At both moderate (WS-M) and severe (WS-S) drought stress conditions, differentially expressed genes were distributed across a broad set of Gene Ontology categories, indicating extensive transcriptional remodeling under water deficit (Figure 3).

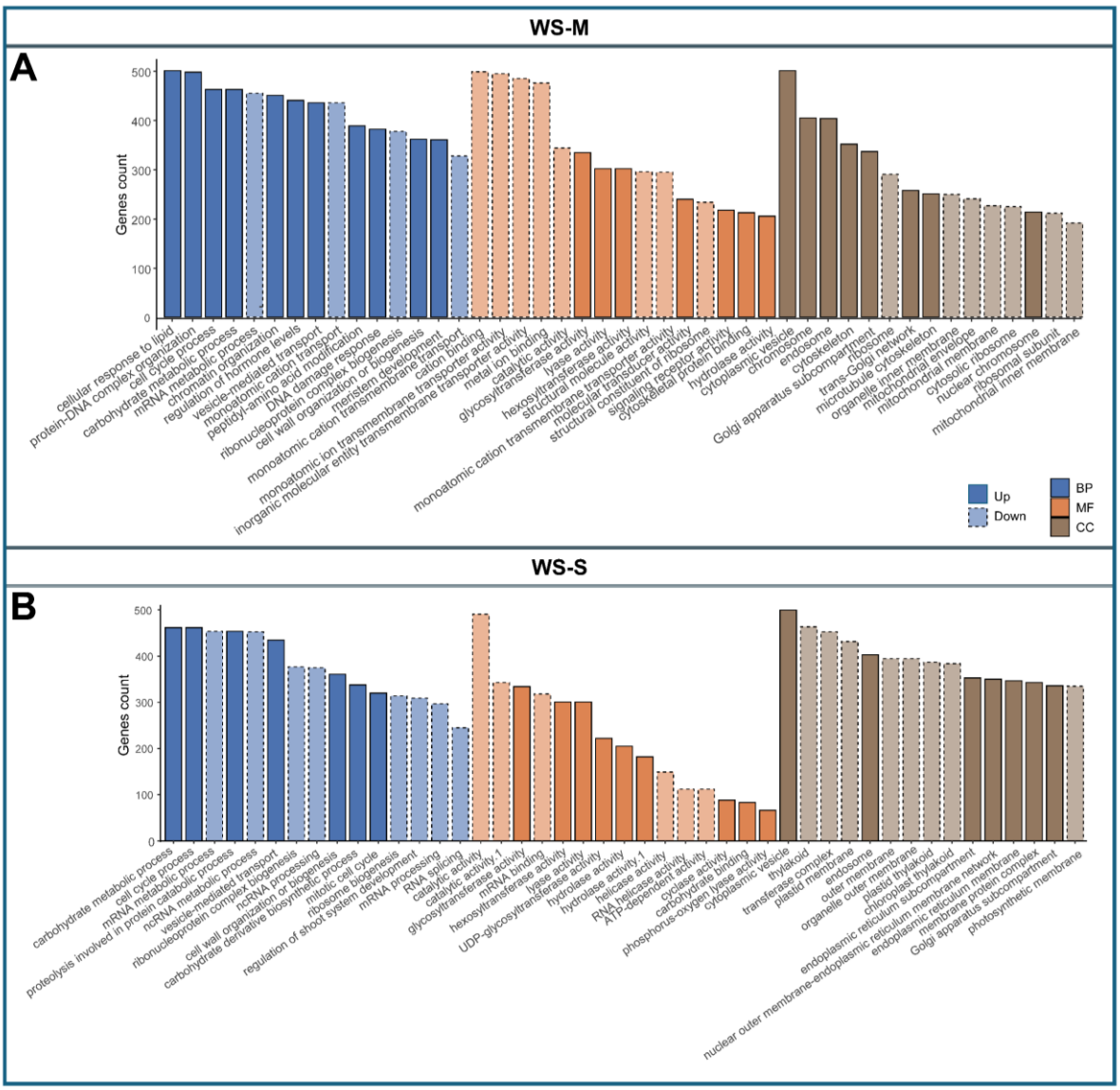

Figure 3. *Bar plots summarize significantly enriched Gene Ontology (GO) terms among differentially expressed genes, separated by GO domain (BP, biological process; MF, molecular function; CC, cellular component) and regulation direction (Up vs Down, as indicated by solid vs dashed bars). The upper and lower panels correspond to the two drought transitions/severity contrasts analyzed (moderate - A - and severe drought - B), highlighting a shift from early regulatory/transport-associated responses to stronger repression of photosynthesis- and growth-related categories and enhanced stress/maintenance-associated functions as drought severity increases.*

Susceptible genotype shows early regulatory rewiring and late stress escalation under increasing drought severity

At the transition from well-watered conditions to moderate drought (T0 to WS-M), the susceptible genotype GPE008940 showed pronounced transcriptional changes (5328 upregulated and 5852 downregulated genes, Figure 4C). Several strongly induced transcripts were associated with drought- and stress-related functions, including an abscisic acid and environmental stress–inducible protein (TAS14), low-temperature-induced proteins, heat shock proteins, and multiple transport-related genes such as aquaporins and sodium-coupled amino acid transporters. In parallel, transcriptional regulators and signaling components, including NAC and homeobox–leucine zipper transcription factors, were

also upregulated. Conversely, a subset of genes related to cell wall components, hormone-regulated proteins, and receptor-like kinases showed significant downregulation at this stage.

During the subsequent transition from moderate to severe drought (WS-M to WS-S), the transcriptional profile shifted toward genes associated with tissue remodeling and late stress responses (1215 upregulated and 1234 downregulated, Figure 4D). Differentially expressed genes included senescence-associated proteases, chitinases, expansins, extensins, and glycine-rich cell wall proteins, indicating extensive modulation of cell wall–related processes. Several enzymes involved in secondary metabolism and redox regulation, such as laccases, dioxygenases, and glutaredoxins, were also differentially expressed. In addition, genes encoding sugar transporters of the SWEET family, hormone-related enzymes, and RNA-binding proteins showed significant regulation, reflecting further reorganization of metabolic and regulatory processes as drought severity increased.

\

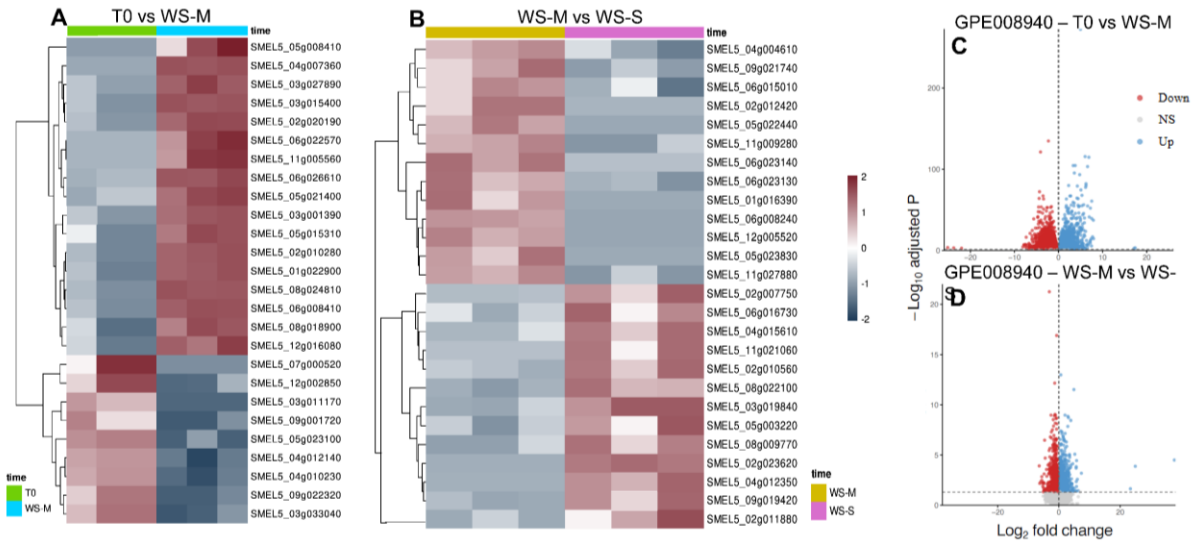

Figure 4. *Heatmaps (left) show scaled expression patterns of representative drought-responsive genes across samples, grouped by genotype and drought severity (A - WS-M and WS-S - B; color bars indicate sample classes). Genes are clustered by similarity, highlighting genotype- and stage-dependent transcriptional trajectories. Volcano plots (right; C–D) summarize differential expression for the corresponding contrasts, with significantly upregulated genes shown in blue, downregulated genes in red, and non-significant genes in grey (dashed lines indicate the applied fold-change and adjusted P-value thresholds).*

Gene set enrichment analysis (GSEA, Figure 5) revealed a marked functional separation between activated and suppressed gene sets during the early drought stage (T0 to WS-M; Figure 4A,B). Among activated biological processes, enrichment was dominated by intracellular transport and localization categories (intracellular protein transport, protein transport, establishment of protein localization), together with processes associated with protein–DNA complex organization and mRNA metabolic process. This pattern was supported by the induction of representative nuclear/RNA-processing components, including a U11/U12 snRNP 35 kDa component (SMEL5_09g024500) and a nuclear export factor SDE5 (SMEL5_07g019890; Table 1). In addition, proteasome- and peptidase-related terms (proteasome complex, peptidase complex) were enriched among activated gene sets, consistent with concurrent regulation of protein turnover pathways; among the high-amplitude DEGs, an EID1-like F-box protein (SMEL5_06g029750; Table 1) exemplified this component of the response. In parallel, a subset of the largest DEGs included regulators linked to light/clock and growth-associated

signaling, including LUX (SMEL5_06g005050), a PIF1-like factor (SMEL5_06g002810), and GA2-oxidase (SMEL5_04g003260; Table 1).

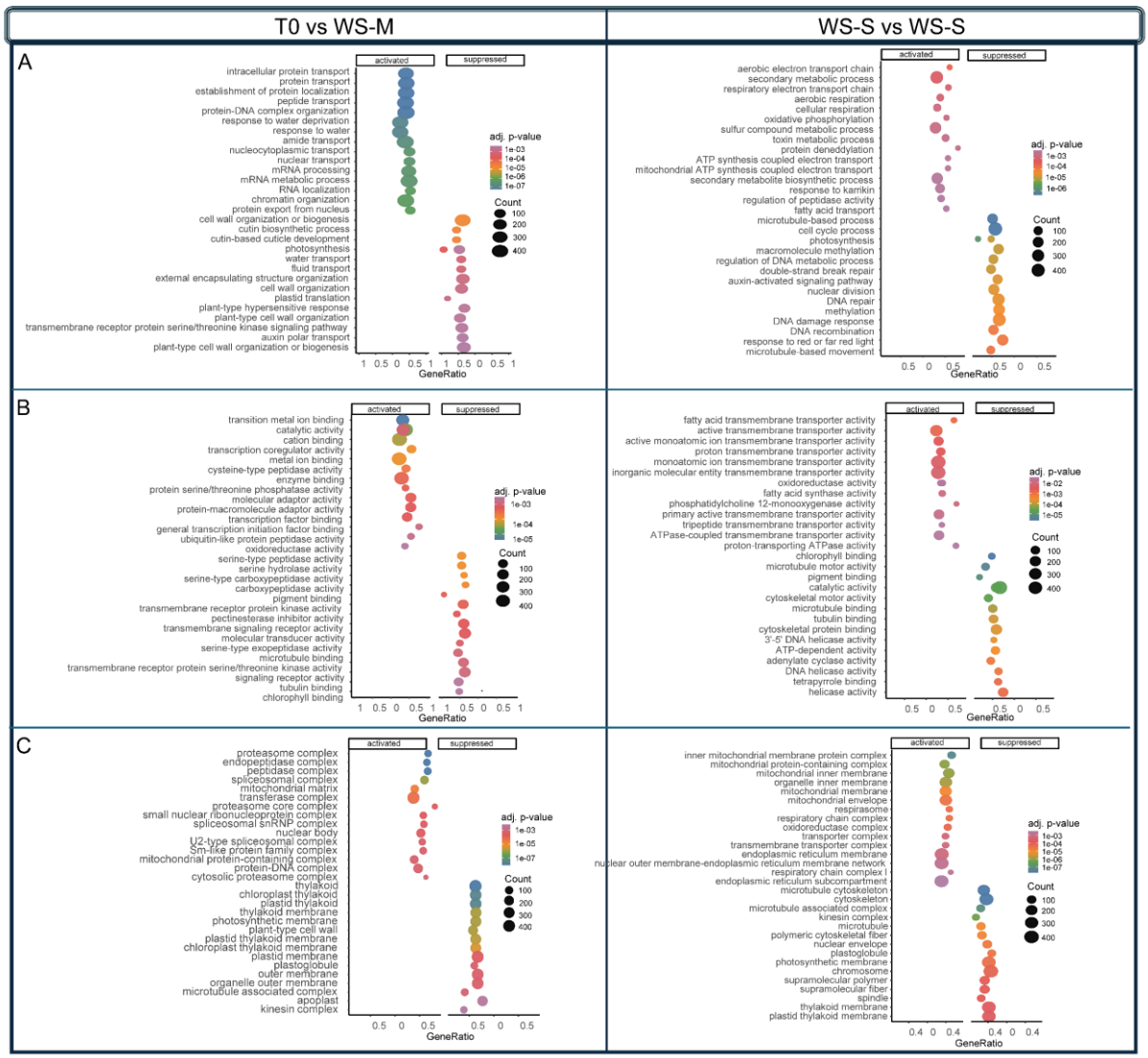

Figure 5. *Dot plots summarize significantly enriched terms among upregulated ("activated") and downregulated ("suppressed") gene sets for each genotype and drought transition (T0 to WS-M and WS-M to WS-S). Panels report enrichment for Biological Process (A), Molecular Function (B), and Cellular Component (C), highlighting coordinated early regulatory and transport-related activation at moderate stress and a stronger suppression of photosynthesis/light-harvesting and growth-associated functions under severe stress, together with activation of mitochondrial respiration, detoxification, and membrane/lipid remodeling pathways. Dot size reflects gene-set size (count) and dot colour indicates adjusted P value.*

Among suppressed biological processes at WS-M, enrichment was primarily associated with structural and growth-related functions, including cell wall organization or biogenesis, cutin-based cuticle development, and photosynthesis. Cuticle-related suppression was mirrored by downregulation of multiple epidermal barrier components, including an ABCG transporter (SMEL5_01g006970), CER3 (SMEL5_07g000910), a wax ester synthase/DGAT11-like enzyme (SMEL5_01g030260), a GPAT5-like gene (SMEL5_11g028180), and a strongly repressed MYB41-like regulator (SMEL5_04g005030;

Table 1). Similarly, chloroplast- and photosynthesis-linked suppression was reflected by decreased expression of photoprotection and plastid maintenance nodes, including an ELIP1-like gene (SMEL5_09g018400), SOQ1 (SMEL5_01g010820/SMEL5_01g010830), a plastid RNA polymerase β′ (SMEL5_11g014820), and an NDH lumenal subunit (SMEL5_04g002050; Table 1). Water-transport categories were also negatively enriched at WS-M, with repression of specific aquaporins (TIP-type RB7-5A, SMEL5_06g014400; NIP2-1-like, SMEL5_05g012270) despite induction of other isoforms (e.g., TIP1-1-like, SMEL5_10g022180; Table 1).

GSEA confirmed a stage-specific functional redistribution at WS-S (Figure 4A,B). Negatively enriched categories were dominated by chlorophyll/pigment binding and photosynthetic light harvesting, mirrored by high-amplitude repression of multiple antenna and PSI loci, including chlorophyll a–b binding protein 21 (SMEL5_02g009770, SMEL5_02g009780), chlorophyll a–b binding protein 6A (SMEL5_05g007920, SMEL5_05g007900), CP24 10B (SMEL5_01g007320), and PSI components such as subunit XI (SMEL5_06g028360) and subunit III (SMEL5_02g011300; Table 1). In parallel, strong negative enrichment for microtubule cytoskeleton-, kinesin complex- and cell cycle–related terms was supported by repression of kinesins (KIN-12B, SMEL5_09g023710; KIN-12F, SMEL5_07g022520; KIN-14I, SMEL5_01g011400), a cyclin-A1-4-like gene (SMEL5_04g010390), tubulins (TUBB2, SMEL5_10g020840; TUA3, SMEL5_05g018500), and a KNOLLE-like syntaxin (SMEL5_06g012380; Table 1). Carbon allocation and tissue remodeling were concurrently affected, exemplified by strong repression of sucrose efflux transporters (SWEET12-like, SMEL5_06g023130; SWEET9-like, SMEL5_06g023140) and wall-associated loci such as expansin-B3-like (SMEL5_04g004610), a pectinesterase-like gene (SMEL5_02g015680), and cellulose synthase-like D5 (SMEL5_09g016950; Table 1).

Conversely, positively enriched gene sets at WS-S were dominated by mitochondrial and maintenance-associated functions, including respirasome/respiratory chain/oxidative phosphorylation/ATP synthesis, supported by induction of an ADP/ATP carrier (SMEL5_05g024330), a NADH–quinone oxidoreductase subunit (SMEL5_03g032040), and an FQR1-like NAD(P)H dehydrogenase (SMEL5_04g005860; Table 1). Severe drought also intensified membrane and chemical stress–associated programs, including lipid remodeling and oxylipin-linked enzymes (PIOX-like, SMEL5_02g027950; FAD2-like desaturases, SMEL5_05g015120, SMEL5_05g015160; PLIP1, SMEL5_01g015930; PLA1-II-like, SMEL5_02g006090), together with detoxification and redox-related components (GST, SMEL5_01g021840; metallothionein-like, SMEL5_04g010990) and conjugation/specialized metabolism enzymes (P450 71AU50-like, SMEL5_05g015090; UGT-like, SMEL5_04g015610; Table 1). Multiple exporters were also induced (ABCG23, SMEL5_03g024080; ABCG10-like, SMEL5_07g019280; PDR1-like, SMEL5_09g022110). Notably, within cuticle-related regulation, a WIN1/SHN-like wax/cuticle regulator (SMEL5_03g026860) was strongly repressed despite induction of ABC/PDR transporters and lipid-transfer associated genes (Table 1).

Table 1. Key drought-responsive genes prioritized in the susceptible genotype GPE008940 across progressive drought severity. The table reports the selected candidate transcripts (gene IDs) highlighted in the Results for the "T0 to WS-M" and "WS-M to WS-S" transitions, with functional annotation, direction of regulation in each contrast, and gene ontology.

Transition	Gene ID	Function	log2FC	GO
T0 to WS-M	SMEL5_07g019890	Nuclear export factor SDE5	1.05	ta-siRNA processing
	SMEL5_06g029750	EID1-like F-box protein	1.72	leaf development
	SMEL5_10g022180	TIP1-1-like aquaporin	2.67	leaf development
	SMEL5_04g003260	GA2-oxidase	3.04	gibberellin biosynthetic process
	SMEL5_06g002810	PIF1-like factor	3.34	gibberellin biosynthetic process
	SMEL5_06g005050	LUX	3.59	regulation of circadian rhythm
	SMEL5_09g024500	U11/U12 snRNP 35 kDa component	3.64	mRNA splicing, via spliceosome
	SMEL5_07g000910	CER3	−1.03	wax biosynthetic process
	SMEL5_01g010820	SOQ1	−1.26	metal ion binding
	SMEL5_01g010830	SOQ1	−1.27	metal ion binding
	SMEL5_06g014400	TIP-type RB7-5A aquaporin	−1.32	water transport
	SMEL5_04g002050	NDH lumenal subunit	−1.43	photosystem I assembly
	SMEL5_11g014820	Plastid RNA polymerase β'	−1.49	DNA-templated transcription
	SMEL5_05g012270	NIP2-1-like aquaporin	−1.55	channel activity
	SMEL5_11g028180	GPAT5-like	−1.66	cutin biosynthetic process
	SMEL5_01g030260	Wax ester synthase / DGAT11-like	−1.73	triglyceride biosynthetic process
	SMEL5_09g018400	ELIP1-like	−2.79	photosynthesis
	SMEL5_01g006970	ABCG transporter	−3.06	response to abscisic acid
	SMEL5_04g005030	MYB41-like regulator	−3.82	response to abscisic acid
WS-M to WS-S	SMEL5_02g006090	PLA1-II-like phospholipase	1.68	phospholipid metabolic process
	SMEL5_04g010990	Metallothionein-like type 2	2.3	metal ion binding
	SMEL5_01g015930	PLIP1 phospholipase A1	2.4	triglyceride biosynthetic process
	SMEL5_09g022110	PDR1-like ABC exporter	2.43	hormone transport
	SMEL5_07g019280	ABCG10-like exporter	2.57	ABC-type transporter activity
	SMEL5_03g032040	NADH–quinone oxidoreductase subunit	2.63	proton transmembrane transport
	SMEL5_03g024080	ABCG23 exporter	2.71	transmembrane transport
	SMEL5_05g015090	P450 71AU50-like	2.84	monooxygenase activity
	SMEL5_04g005860	FQR1-like NAD	2.89	NADPH dehydrogenase (quinone) activity
	SMEL5_01g021840	GST glutathione S-transferase	2.89	glutathione transferase activity
	SMEL5_05g015160	FAD2-like desaturase	2.92	unsaturated fatty acid biosynthetic process
	SMEL5_05g015120	FAD2-like desaturase	2.96	unsaturated fatty acid biosynthetic process
	SMEL5_05g024330	ADP/ATP carrier, mitochondrial	3.24	mitochondrial ADP transmembrane transport
	SMEL5_02g027950	PIOX-like alpha-dioxygenase	4.04	response to oxidative stress
	SMEL5_04g015610	UGT-like glucosyltransferase	5.73	negative regulation of fatty acid metabolic process
	SMEL5_05g018500	TUA3 tubulin alpha-3	−1.03	microtubule cytoskeleton organization
	SMEL5_02g011300	PSI subunit III	−1.06	photosynthesis
	SMEL5_06g028360	PSI reaction center subunit XI	−1.21	photosynthesis
	SMEL5_10g020840	TUBB2 tubulin beta-2	−1.47	structural constituent of cytoskeleton
	SMEL5_05g007900	Chlorophyll a–b binding protein 6A	−2.06	photosynthesis, light harvesting in photosystem I
	SMEL5_01g011400	KIN-14I kinesin-like protein	−2.16	oxidoreductase activity
	SMEL5_01g007320	CP24 10B	−2.24	photosynthesis, light harvesting in photosystem I
	SMEL5_07g022520	KIN-12F kinesin-like protein	−2.34	microtubule-based movement
	SMEL5_05g007920	Chlorophyll a–b binding protein 6A	−2.42	photosynthesis, light harvesting in photosystem I
	SMEL5_09g016950	Cellulose synthase-like D5	−2.44	cellulose biosynthetic process
	SMEL5_02g009780	Chlorophyll a–b binding protein 21	−2.48	response to desiccation
	SMEL5_04g010390	Cyclin-A1-4-like	−2.76	Cell division
	SMEL5_09g023710	KIN-12B kinesin-like protein	−2.77	microtubule-based movement
	SMEL5_02g009770	Chlorophyll a–b binding protein 21	−2.91	response to desiccation
	SMEL5_03g026860	WIN1/SHN-like wax/cuticle regulator	−3.15	triglyceride biosynthetic process
	SMEL5_06g012380	KNOLLE-like syntaxin	−3.57	cell division
	SMEL5_02g015680	Pectinesterase-like	−4.21	cell wall modification
	SMEL5_04g004610	Expansin-B3-like	−4.89	Cell wall biogenesis/degradation
	SMEL5_06g023140	SWEET9-like sucrose efflux transporter	−5.08	carbohydrate transport
	SMEL5_06g023130	SWEET12-like sucrose efflux transporter	−6.47	carbohydrate transport

Tolerant genotype shows ABA-centred early protection and controlled acclimation under increasing drought severity

In the tolerant genotype GPE020510, drought stress induced distinct and stage-dependent transcriptional changes during both the transition from well-watered conditions to moderate drought (T0 to WS-M) and from moderate to severe drought (WS-M to WS-S). At the moderate drought stage (T0 to WS-M), GPE020510 displayed differential regulation of a specific subset of genes (5925 upregulated and 6807 downregulated, Figure 6C), suggesting rapid engagement of dehydration-responsive protection, transport homeostasis, and redox buffering.

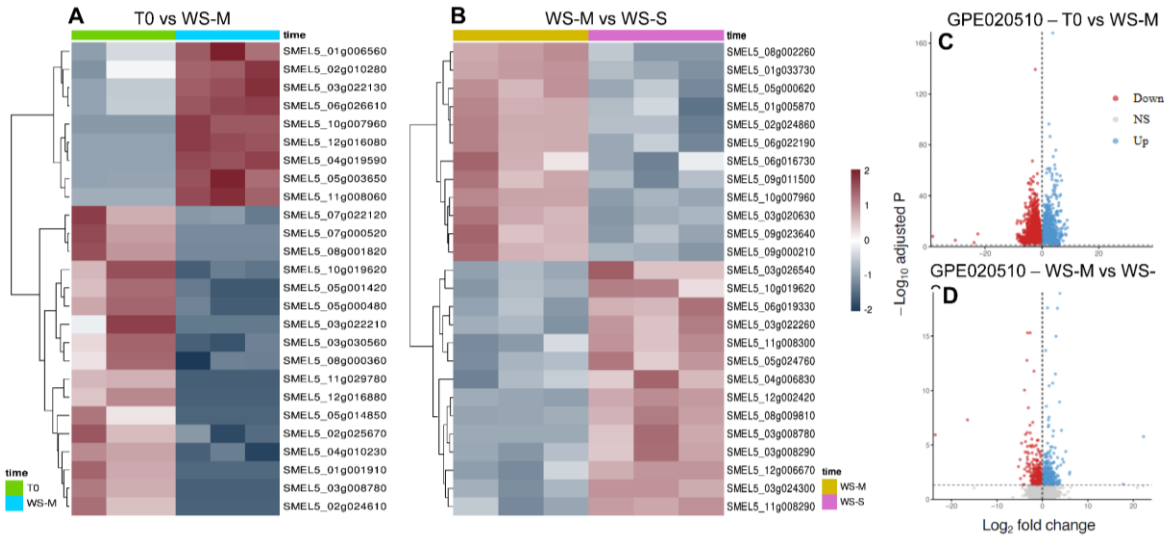

Figure 6. *Stage-specific differential expression in response to progressive drought. Heatmaps (left) show scaled expression patterns of representative drought-responsive genes across samples, grouped by genotype and drought severity (A, T0 to WS-M; B, WS-M to WS-S; colour bars indicate sample classes). Genes are clustered by similarity, highlighting genotype- and stage-dependent transcriptional trajectories. Volcano plots (right) summarize differential expression for the corresponding contrasts (C, T0 vs WS-M; D, WS-M vs WS-S), with significantly upregulated genes shown in blue, downregulated genes in red, and non-significant genes in grey (dashed lines indicate the applied fold-change and adjusted P-value thresholds).*

Among the most strongly induced transcripts were canonical ABA/dehydration regulators and effectors, including ABI5 (SMEL5_09g001060) and TAS14 (SMEL5_02g020190), together with prominent cellular protectants such as LEA/LEA2-like proteins (SMEL5_03g026640; SMEL5_01g002530) and Rab25-like dehydrin (SMEL5_02g003520) (Table 2). This ABA-centred response was accompanied by induction of additional stress-responsive regulators, including ATHB-7 (SMEL5_08g024810), a ZAT4-like zinc finger (SMEL5_01g019030), and an ERF2-like transcription factor (SMEL5_08g019370). In parallel, moderate drought in GPE020510 was characterized by prominent activation of transport and membrane homeostasis components, including a sodium-coupled neutral amino acid transporter (SMEL5_06g008410) and induced ABCG transporters (SMEL5_01g006930; SMEL5_11g019430), together with redox/detox-associated genes such as ETHE1 (SMEL5_10g004650) and a peroxygenase-like enzyme (SMEL5_05g021400), and a strongly induced low-temperature-induced 65 kDa protein-like transcript (SMEL5_03g015400) (Table 2). Concomitantly, the WS-M transition also included marked repression of growth-associated outputs, exemplified by multiple auxin-responsive SAUR68-like loci (SMEL5_11g009750; SMEL5_11g001820) and wall-associated genes such as a cellulose synthase-like locus

(SMEL5_07g013090) and a polygalacturonase-like gene (SMEL5_03g010400) (Table 2). During the subsequent transition to severe drought (WS-M to WS-S), the transcriptional profile of GPE020510 shifted toward a broader involvement of stress acclimation and remodeling-related genes (742 upregulated and 556 downregulated, Figure 6D), with prominent signatures linked to plastid/light management and proteostasis. Induced photoprotection and light-handling nodes included ELIP1 (SMEL5_09g018430), OHP2 (SMEL5_05g017260), and BIC1/BIC1-like regulators (SMEL5_12g014390; SMEL5_12g014380) (Table 2). Severe drought was also associated with activation of dehydration/cold-related regulators and chaperone capacity, including DREB1A-like (SMEL5_03g014860), CBF/AP2 (SMEL5_03g014870), and small heat shock proteins (SMEL5_12g006670; SMEL5_03g017990) (Table 2). In parallel, GPE020510 showed induction of genes compatible with targeted metabolic adjustment, including carbohydrate- and lipid-associated drivers such as β-amylase 3 (SMEL5_08g000360), 6-phosphofructokinase 6-like (SMEL5_08g011260), phospholipase A1-II 1-like (SMEL5_02g006090), and a FAD2 desaturase (SMEL5_05g024580), alongside stress-linked oxidative and specialized metabolism enzymes including F6H1-3 (SMEL5_05g024760), premnaspirodiene oxygenase (SMEL5_11g013170), CYP94B3-like/CYP98A2-like (SMEL5_03g021570), and SMEL5_06g017490 (Table 2). Notably, this late phase also included selective repression of specific nodes, including PLIP1 (SMEL5_01g015930), KAT3 (SMEL5_08g007330), and a WRKY70-like factor (SMEL5_10g019970) (Table 2).

Table 2. *Key drought-responsive genes prioritized in the tolerant genotype GPE020510 across progressive drought severity. The table reports the selected candidate transcripts (gene IDs) highlighted in the Results for the "T0 to WS-M" and "WS-M to WS-S" transitions, with functional annotation, direction of regulation in each contrast, and gene ontology.*

Transition	Gene ID	Function	log2FC	GO
T0 to WS-M	SMEL5_01g002530	LEA/LEA2-like protein	4.8	response to water deprivation
	SMEL5_08g019370	ERF2-like transcription factor	5.12	ethylene-activated signaling pathway
	SMEL5_02g003520	Rab25-like dehydrin	5.13	response to water deprivatio
	SMEL5_05g021400	Peroxygenase-like enzyme	5.15	monooxygenase activity
	SMEL5_10g004650	ETHE1	5.2	glutathione metabolic process
	SMEL5_08g024810	ATHB-7	5.21	response to water deprivation
	SMEL5_11g019430	ABCG transporter	5.64	response to abscisic acid
	SMEL5_01g006930	ABCG transporter	5.68	response to abscisic acid
	SMEL5_01g019030	ZAT4-like zinc finger	5.84	regulation of DNA-templated transcription
	SMEL5_03g026640	LEA/LEA2-like protein	5.95	response to water deprivation
	SMEL5_02g020190	TAS14	6.32	response to water deprivation
	SMEL5_09g001060	ABI5	6.59	response to water deprivation
	SMEL5_06g008410	Sodium-coupled neutral amino acid transporter	6.74	amino acid transmembrane transport
	SMEL5_03g015400	Low-temperature-induced 65 kDa protein-like	6.94	response to stress
	SMEL5_07g013090	Cellulose synthase-like locus	−5.26	plant-type primary cell wall biogenesis
	SMEL5_03g010400	Polygalacturonase-like gene	−5.73	plant-type cell wall modification
	SMEL5_11g001820	SAUR68-like auxin-responsive gene	−6.43	response to auxin
	SMEL5_11g009750	SAUR68-like auxin-responsive gene	−6.55	response to auxin
WS-M to WS-S	SMEL5_05g017260	OHP2	1.05	photosystem II assembly
	SMEL5_09g018430	ELIP1	1.89	photosynthesis
	SMEL5_12g014380	BIC1/BIC1-like regulator	1.93	blue light signaling pathway
	SMEL5_12g014390	BIC1/BIC1-like regulator	2.03	blue light signaling pathway
	SMEL5_08g011260	6-phosphofructokinase 6-like	2.07	fructose 6-phosphate metabolic process
	SMEL5_05g024580	FAD2 desaturase	2.15	unsaturated fatty acid biosynthetic process
	SMEL5_06g017490	Stress-linked oxidative/specialized metabolism enzyme	2.35	cellular response to hydrogen peroxide
	SMEL5_02g006090	Phospholipase A1-II 1-like	2.45	lipid catabolic process
	SMEL5_03g021570	CYP94B3-like / CYP98A2-like	2.72	jasmonic acid metabolic process
	SMEL5_08g000360	β-amylase 3, chloroplastic	2.9	starch catabolic process
	SMEL5_03g014870	CBF/AP2	3.14	DNA-binding transcription factor activity
	SMEL5_11g013170	Premnaspirodiene oxygenase	3.27	monooxygenase activity
	SMEL5_03g017990	Small heat shock protein	3.36	Stress response
	SMEL5_03g014860	DREB1A-like	3.47	Stress response
	SMEL5_05g024760	F6H1-3	3.63	phenylpropanoid biosynthetic process
	SMEL5_12g006670	Small heat shock protein	3.99	Stress response
	SMEL5_10g019970	WRKY70-like factor	−2.05	ethylene-activated signaling pathway
	SMEL5_08g007330	KAT3	−2.27	potassium ion transmembrane transport
	SMEL5_01g015930	PLIP1	−3.44	Biological Process

Gene set enrichment analysis of differentially expressed genes revealed stage-dependent functional enrichment patterns during the progression from well-watered conditions to moderate (WS-M) and severe drought (WS-S - Figure 7). At the early drought stage (T0 to WS-M), enrichment profiles showed a clear separation between gene sets associated with up-regulated and down-regulated transcripts. Within the Biological Process ontology at WS-M, up-regulated gene sets were predominantly associated with catabolic and respiratory processes, including carboxylic and organic acid catabolism, amino acid catabolism, small molecule catabolic process, and cellular respiration, together with regulation of proteolysis, lipid catabolic processes, and ribosomal small subunit biogenesis. In contrast, down-regulated biological processes were mainly related to photosynthesis and structural components, including cell wall organization or biogenesis, cutin-based cuticle development, water transport, and auxin polar transport. Consistent patterns were observed across the Molecular Function and Cellular Component ontologies. At WS-M, up-regulated gene sets were enriched for ion binding and transmembrane transporter activities, together with DNA- and protein-related catalytic functions, whereas down-regulated molecular functions included chlorophyll and pigment binding. At the cellular level, up-regulated gene sets were associated with protein- and degradation-related complexes, including proteasome- and spliceosome-associated components, while down-regulated gene sets were enriched for plastid- and photosynthesis-related compartments such as thylakoid membranes and plastoglobules.

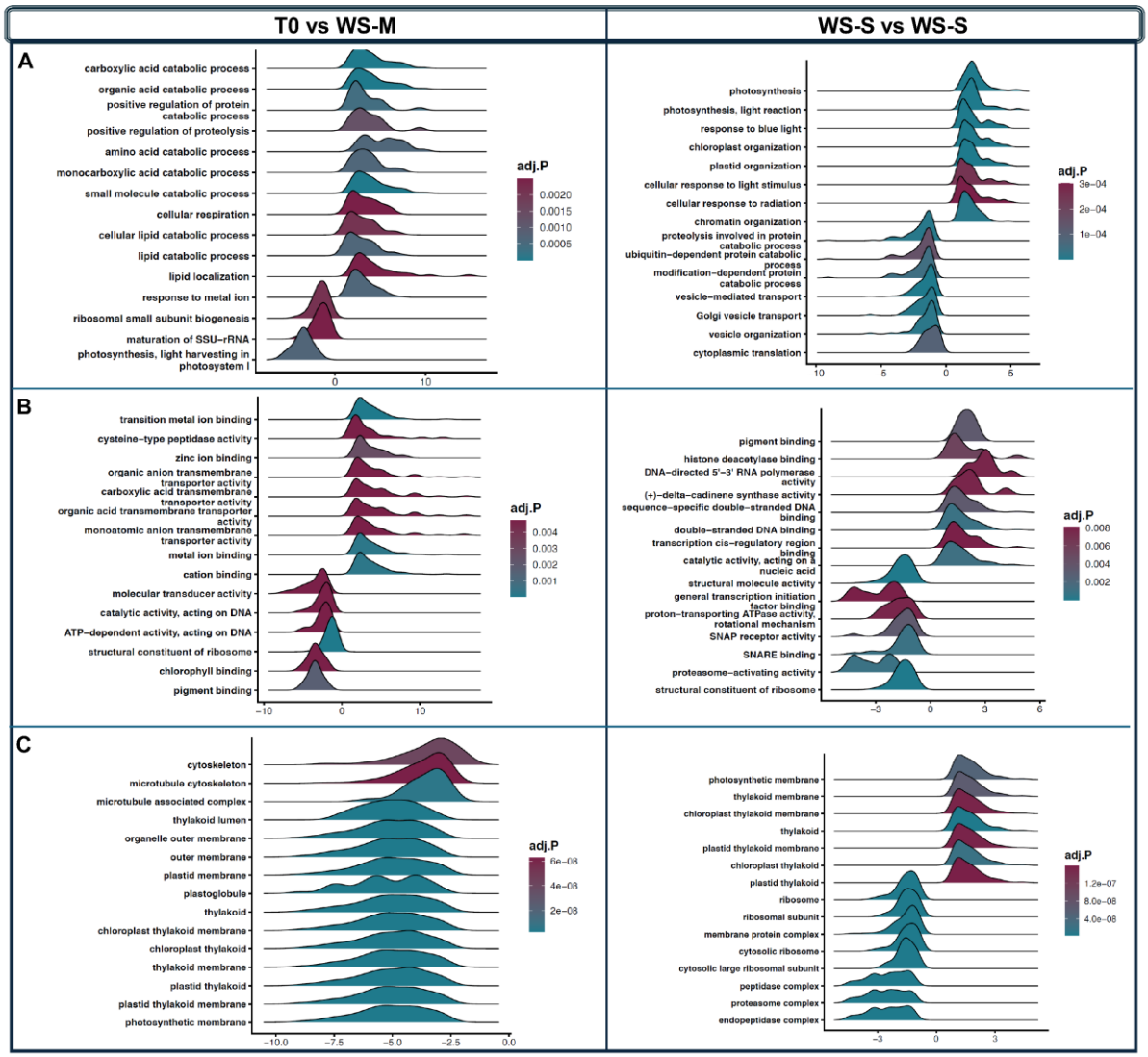

Figure 7. *Ridge plots of gene set enrichment results across progressive drought in the tolerant genotype. Enriched terms are shown for Biological Process (top row), Molecular Function (middle row) and Cellular Component (bottom row). The left column summarizes the transition from well-watered to moderate drought (T0 to WS-M), while the right column summarizes the transition from moderate to severe drought (WS-M to WS-S). For each panel, ridges represent individual significantly enriched terms, positioned along the enrichment score axis (positive values indicate enrichment among upregulated gene sets; negative values indicate enrichment among downregulated gene sets). Ridge colour encodes the adjusted P value (adj. P).*

Co-expression modules associated with moderate-to-severe drought transition

Comparison of differentially expressed genes between the two genotypes at comparable drought stages revealed a very limited overlap. To further characterize transcriptional changes associated with the transition from T0 to severe drought, we performed a weighted gene co-expression network analysis (WGCNA) using samples collected at comparable physiological stages. This approach was employed to identify groups of co-expressed genes whose coordinated behavior differed between genotypes during the progression to severe water deficit (Figure 8).

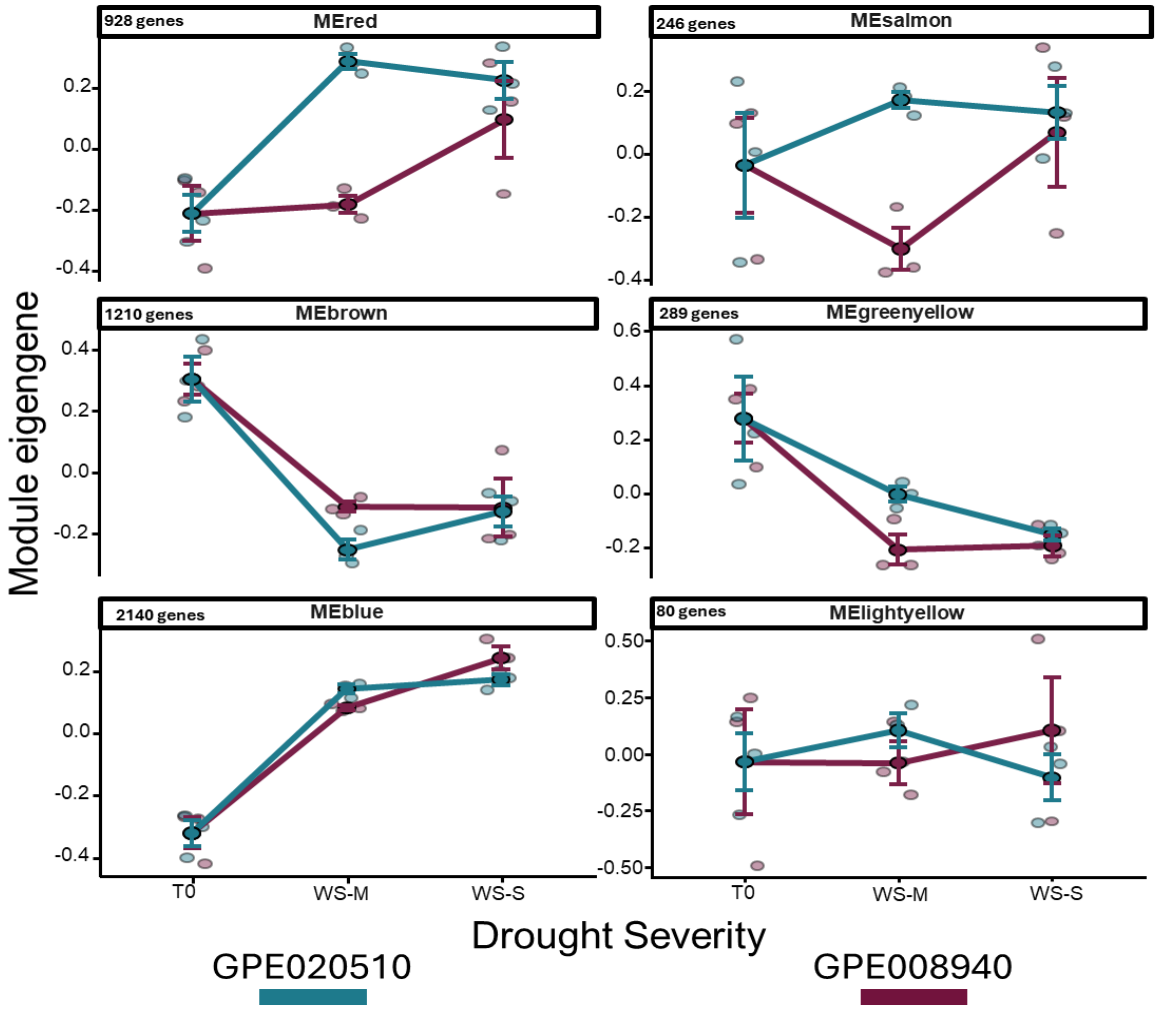

Figure 8. *Eigengene trajectories of six WGCNA modules across increasing drought severity (T0 to WS-S) in the two genotypes. For each module, individual sample eigengene values are shown as points, and group means ± error are indicated by larger points with error bars, and genes per module are reported.*

Six co-expression modules showed distinct eigengene trajectories across drought progression and differed between genotypes (Figure 8). Hub genes are listed in Supplementary Table 1. The red module

increased strongly from T0 to WS-M in the tolerant genotype GPE020510 and remained high at WS-S, whereas in the susceptible genotype GPE008940 increased mainly at WS-S. Based on its hubs, this module is consistent with a regulatory/signaling timing program. Hub genes included SMEL5_05g017420 (WRKY51-like), SMEL5_06g018620 (ELF3-like), SMEL5_09g002410 (zinc finger 593-like), and SMEL5_02g020630 (epoxide hydrolase 4-like). The salmon module diverged between genotypes at WS-M: GPE008940 strongly decreased at WS-M and recovered by WS-S, whereas GPE020510 slightly increased at WS-M and remained positive at WS-S. Its hubs point to a membrane trafficking and secondary-metabolism/stress-marker program. Hub genes included SMEL5_01g036930 (syntaxin-121-like Qa-SNARE), SMEL5_05g015090 (P450 71AU50-like), SMEL5_01g004620 (scopoletin glucosyltransferase-like UGT), and SMEL5_06g000430 (SAG21-like). The brown module decreased sharply from T0 to WS-M in both genotypes and remained low at WS-S, with a stronger drop at WS-M in the tolerant genotype GPE020510 and partial recovery by WS-S. Its hub composition points to a chloroplast redox / tetrapyrrole /photosynthetic adjustment program. Representative hub genes included SMEL5_09g000310 (porphobilinogen deaminase), SMEL5_10g025240 (NTRC), and SMEL5_12g004410 (NDH lumenal subunit). The greenyellow module showed a strong reduction from T0 to WS-M followed by persistently low values at WS-S, with a more pronounced WS-M decrease in the susceptible genotype GPE008940 than in the tolerant genotype GPE020510. Its hubs suggest a PRR-like receptor kinases and Ca^{2+}-linked signaling program. Hub genes included SMEL5_08g014220 and SMEL5_08g014230 (AED1-like aspartyl proteases), and receptor-kinase loci SMEL5_11g026670 (EFR-like) and SMEL5_11g025890 (Xa21-like). The blue module increased from T0 to WS-M in both genotypes and further increased toward WS-S, with higher WS-S values in the susceptible GPE008940 than in the tolerant GPE020510. Its hubs are consistent with a core escalation program involving ion/transport and RNA processing/signaling. Hub genes included SMEL5_05g010420 (plasma membrane H+-ATPase 1), SMEL5_01g011740 (SR30-like splicing factor), and SMEL5_10g012140 (VIP1-like). Finally, the lightyellow module displayed opposite trajectories between genotypes: the tolerant GPE020510 increased at WS-M and decreased at WS-S, whereas the susceptible GPE008940 remained near baseline at WS-M and increased at WS-S. Its hub genes support a transcription/translation and regulatory-complex program. Hub genes included SMEL5_12g003930 (SKP1-like 1B), SMEL5_06g024510 (RNA polymerase II subunit 4), SMEL5_02g014660 (eIF3J-A), and SMEL5_04g006610 (SOC1-like).

Discussion

Physiological measurements conducted in this study (*i.e.*: stomatal conductance and leaf water potential, Fig. 1) confirmed the contrasting drought performance under progressive stress previously described within the G2P-SOL framework, with the genotype GPE020510 maintaining plant water status and stomatal function longer than the genotype GPE008940, suggesting improved drought tolerance (Asargew et al., 2024; Lu et al., 2020). At the transcriptome level, both genotypes showed strong reprogramming all over the period, with responses staged across WS-M and WS-S, defined for each genotype by comparable leaf water potential.

Under moderate stress (WS-M), the tolerant genotype GPE020510 was characterized by signatures points to early acclimation, including metabolic adjustment and ABA-linked regulatory control. This aligns with a well-established framework in which ABA-centred signaling and downstream effectors coordinate early dehydration responses that promote osmotic adjustment, cellular protection and homeostasis buffering (Liao et al., 2023; Soma et al., 2021; Wei et al., 2025). In our data, this early protective configuration is supported by candidate regulators/effectors such as ABI5 (SMEL5_09g001060) and TAS14 (SMEL5_02g020190), together with dehydration-associated

protectants (*e.g.*, LEA/dehydrin-type loci; Table 2), core components of drought-responsive transcriptional cascades (Muñoz-Mayor et al., 2012; Skubacz et al., 2016; Vaseva et al., 2025). Importantly, the tolerant profile at WS-M also included growth restraint (*e.g.*, repression of SAUR-associated loci and wall-related genes), which is coherent with the broader concept that drought acclimation often requires prioritizing protection overgrowth through hormone-mediated reallocation (Jiang et al., 2025; Khan et al., 2023; Seleiman et al., 2021). In contrast, at WS-M the susceptible genotype GPE008940 showed a response biased toward regulatory rewiring, with enrichment for RNA/nuclear and turnover-associated functions, in line with reported transcript fate and protein composition changes under stress conditions (Irshad and Sharma, 2024). However, in the susceptible genotype GPE008940 this regulatory engagement coincided with an early downshift of two protective "infrastructure" layers: epidermal barrier/cuticle-associated programs and chloroplast/light-harvesting and plastid maintenance functions (Figures 4–5; Table 1). This is biologically meaningful because cuticle and wax pathways have been linked to limiting non-stomatal water loss and mitigating dehydration-associated injury (Chen et al., 2020; Han et al., 2026; Zhao et al., 2025), while chloroplast photoprotection and plastid gene-expression/maintenance are central to preventing excess excitation pressure and ROS build-up as CO_2 supply declines under drought (Didaran et al., 2024; Gao et al., 2026; Martins et al., 2023; S. Wang et al., 2025). Thus, the susceptible genotype appears to enter the trajectory toward severe stress with comparatively weaker deployment of barrier- and plastid-support outputs, plausibly increasing vulnerability to downstream homeostasis loss.

As drought intensified to WS-S, the susceptible genotype adopted a transcriptional configuration consistent with a low carbon gain/high maintenance state: strong repression of light harvesting and growth-related machinery together with increased representation of mitochondrial respiration, detoxification, membrane/lipid remodeling and transporter/export functions (Figures 4–5). This pattern matches widely described late drought physiology in which reduced photosynthetic productivity co-occurs with increased energetic and biochemical costs associated with damage control, redox management, and membrane maintenance (Chachar et al., n.d.; Chauhan et al., 2023; Nour et al., 2024; Qiao et al., 2024). By contrast, the tolerant genotype GPE020510 showed a more controlled severe-stress profile, with evidence of plastid/light-management and proteostasis-related adjustment and a more targeted metabolic response, mechanisms known for their role in stress regulations and mitigation (Cheng et al., 2025; Li et al., 2026; S. Wang et al., 2025; Wei et al., 2020). Together, the two-stage comparison supports the interpretation that susceptibility here reflects coordination and timing: early regulatory rewiring coupled to reduced barrier/plastid-support signatures, followed by stronger late maintenance/detox escalation, rather than a simple attenuation of the tolerant program.

WGCNA provided module-level support for the early/late phasing model (Figure 8), hub genes are listed in Supplementary Table X. A first axis involves regulatory/stress-signaling and membrane/trafficking modules that separate at WS-M. The red module rises early in the tolerant genotype GPE020510 and remains elevated, whereas the susceptible GPE008940 shows a stronger increase mainly at WS-S. Its hub composition is consistent with a coordinated stress-regulatory program integrating hormone-linked control, osmotic adjustment and redox/proteostasis components (Abbas et al., 2023; Ali et al., 2025; Jurado-Mañogil et al., 2024). In parallel, the salmon module highlights a membrane-centered branch of the response, with hubs including a SYP121/PEN1-class syntaxin (SMEL5_01g036930) together with lipid/secondary-metabolism and stress-marker nodes. Given the established role of SYP121/PEN1-class SNAREs in secretory traffic and guard-cell/stomatal function (Eisenach et al., 2012), these trajectories suggest that the tolerant GPE020510 engages trafficking-linked adjustment earlier, while the susceptible GPE008940 shows a delayed or differently phased deployment of the same module. A second axis emerging from the co-expression structure is

plastid/redox-centered regulation. The brown module is enriched in chloroplast and redox/tetrapyrrole-linked hubs, including NTRC (SMEL5_10g025240), porphobilinogen deaminase (SMEL5_09g000310) and additional chloroplast redox and photoprotective components. The trajectory shows a pronounced shift already at WS-M (stronger in the tolerant genotype, with partial recovery toward WS-S), compatible with early tuning of chloroplast redox/energy metabolism and tetrapyrrole-linked processes (Karami et al., 2025; Nagahatenna et al., 2015; Suzuki et al., 2012; S. Wang et al., 2025), potentially limiting downstream ROS amplification during drought escalation. Beyond these core axes, the greenyellow module points to genotype-dependent modulation of a receptor/Ca^{2+}/protease signaling layer. Its stronger downshift in GPE008940 suggests differential prioritization of this signaling program during stress entry, consistent with drought–defense cross-talk and resource-allocation trade-offs (Dwivedi et al., 2021; Leisner et al., 2023). In addition to these core axes, two modules capture broader reprogramming layers that become more apparent with drought escalation. The blue module shows a progressive increase from T0 to WS-M and further toward WS-S in both genotypes but reaches higher values under WS-S in the susceptible GPE008940. Its hub composition suggests a coordinated "core drought-coping" program integrating osmotic/ABA-linked responses, ion and membrane energization, redox buffering, and proteostasis/autophagy (Bandurska, 2022; De Rossi et al., 2021; Dreyer et al., 2024; Haghpanah et al., 2024; Muhammad Aslam et al., 2022; Refaiy et al., 2026; M. Wang et al., 2025; Yu et al., 2025). In contrast, the lightyellow module displays opposite temporal phasing between genotypes: it increases at WS-M and then declines toward WS-S in the tolerant GPE020510, whereas the susceptible GPE008940 remains closer to baseline at WS-M and increases mainly at WS-S. Notably, lightyellow is a small module (80 genes), so functional interpretation should be carefully evaluated. This module points to a compact transcription/translation and regulatory-complex program whose deployment is earlier in the tolerant genotype but shifted toward late-stage induction in the susceptible genotype, in line with a stronger requirement for severe-stage reprogramming as drought reaches WS-S.

Integrating DEG/GSEA with module-level trajectories supports a model in which drought tolerance in GPE020510 relies on earlier, coordinated acclimation, particularly plastid/redox and membrane-regulatory tuning, thereby dampening the need for broad late-stage maintenance and remodeling responses that dominate in GPE008940 at WS-S.

Conclusion

This study provides a stage-resolved transcriptomic framework for progressive drought in eggplant, showing that tolerance and susceptibility differ in the coordination of regulatory and organelle-/barrier-centered programs across transitions rather than in response magnitude alone. The resulting gene-set and co-expression architecture defines a prioritized set of candidate processes and hub nodes and, critically, anchors them to specific drought stages. A logical extension will be to integrate these stage-specific signatures into genetic mapping and molecular breeding pipelines (*e.g.* by intersecting candidate genes/modules with QTL/association signals, developing informative molecular markers, and deploying them in marker-assisted selection) while leveraging a compact set of complementary physiological and anatomical readouts (plastid/redox stability, carbon balance, barrier integrity) to support validation and refine prioritization across genetic backgrounds and environments.

Author contributions

M.M: Writing – review & editing, Writing – original draft, Visualization, Methodology, Investigation, Formal analysis, Data curation, Conceptualization; **C.M**: Writing – review & editing, Writing – original draft, Visualization, Methodology, Investigation, Formal analysis, Data curation, Conceptualization; **A.M**: Writing – review & editing, Visualization, Conceptualization; **A.M.M**.: Writing – review & editing, Methodology, Formal analysis ; **L.B**: Writing – review & editing, Methodology, Investigation; **A.A**. : Writing – review & editing, Methodology, Investigation; **C.C**: Writing – review & editing, Methodology, Investigation, Conceptualization; **F.S**: Writing – review & editing, Methodology, Investigation, Conceptualization; **E.P**: Writing – review & editing, Methodology, Investigation, Conceptualization.

Funding

The overall work fulfils some goals of the Agritech National Research Center and received funding from the European Union Next-Generation EU (PIANO NAZIONALE DI RIPRESA E RESILIENZA (PNRR)–MISSIONE 4 COMPONENTE 2, INVESTIMENTO 1.4—D.D. 1032 17/06/2022, CN00000022). This study represents a paper within Spoke 4 (Task4.1.1.) 'Next-generation genotyping and -omics technologies for the molecular prediction of multiple resilient traits in crop plants'.

Conflict of interest

The authors declare that the research was conducted in the absence of any commercial or financial relationships that could be construed as a potential conflict of interest.

Data availability

Sequencing data used in this study are openly available in the NCBI database (PRJ _____).

References

1. Abbas, K., Li, J., Gong, B., Lu, Y., Wu, X., Lü, G., Gao, H., 2023. Drought Stress Tolerance in Vegetables: The Functional Role of Structural Features, Key Gene Pathways, and Exogenous Hormones. Int J Mol Sci 24, 13876. https://doi.org/10.3390/ijms241813876
2. Abbass, K., Qasim, M.Z., Song, H., Murshed, M., Mahmood, H., Younis, I., 2022. A review of the global climate change impacts, adaptation, and sustainable mitigation measures. Environ Sci Pollut Res 29, 42539–42559. https://doi.org/10.1007/s11356-022-19718-6
3. Ahluwalia, O., Singh, P.C., Bhatia, R., 2021. A review on drought stress in plants: Implications, mitigation and the role of plant growth promoting rhizobacteria. Resources, Environment and Sustainability 5, 100032. https://doi.org/10.1016/j.resenv.2021.100032
4. Ali, S., Tahir, S., Hassan, S.S., Lu, M., Wang, X., Quyen, L.T.Q., Zhang, W., Chen, S., 2025. The Role of Phytohormones in Mediating Drought Stress Responses in Populus Species. Int J Mol Sci 26, 3884. https://doi.org/10.3390/ijms26083884
5. Araus, J.L., Kefauver, S.C., 2018. Breeding to adapt agriculture to climate change: affordable phenotyping solutions. Current Opinion in Plant Biology, AGRI 2017 45, 237–247. https://doi.org/10.1016/j.pbi.2018.05.003

6. Asargew, M.F., Masutomi, Y., Kobayashi, K., Aono, M., 2024. Water stress changes the relationship between photosynthesis and stomatal conductance. Science of The Total Environment 907, 167886. https://doi.org/10.1016/j.scitotenv.2023.167886
7. Bandurska, H., 2022. Drought Stress Responses: Coping Strategy and Resistance. Plants (Basel) 11, 922. https://doi.org/10.3390/plants11070922
8. Benjamini, Y., Hochberg, Y., 1995. Controlling the False Discovery Rate: A Practical and Powerful Approach to Multiple Testing. Journal of the Royal Statistical Society. Series B (Methodological) 57, 289–300.
9. Blanchard-Gros, R., Bigot, S., Martinez, J.-P., Quinet, M., 2022. Comparison of drought and heat resistance strategies between Solanum lycopersicum and its wild relative Solanum chilense. Presented at the Solanaceae 2022.
10. Chachar, S., Ahmed, N., Hu, X., n.d. Drought-induced aesthetic decline and ecological impacts on ornamentals: mechanisms of damage and innovative strategies for mitigation. Plant Biology n/a. https://doi.org/10.1111/plb.70074
11. Chauhan, J., Prathibha, M., Singh, P., Choyal, P., Mishra, U.N., Saha, D., Kumar, R., Anuragi, H., Pandey, S., Bose, B., Mehta, B., Dey, P., Dwivedi, K.K., Gupta, N.K., Singhal, R.K., 2023. Plant photosynthesis under abiotic stresses: Damages, adaptive, and signaling mechanisms. Plant Stress 10, 100296. https://doi.org/10.1016/j.stress.2023.100296
12. Chen, M., Zhu, X., Zhang, Y., Du, Z., Chen, X., Kong, X., Sun, W., Chen, C., 2020. Drought stress modify cuticle of tender tea leaf and mature leaf for transpiration barrier enhancement through common and distinct modes. Sci Rep 10, 6696. https://doi.org/10.1038/s41598-020-63683-4
13. Cheng, S., Xu, J., Wu, S., Li, Q., Mi, J., 2025. Plant chloroplast stress response: insights from mass spectrometry metabolites analysis. Front. Plant Sci. 16. https://doi.org/10.3389/fpls.2025.1549156
14. Dai, A., 2013. Increasing drought under global warming in observations and models. Nature Clim Change 3, 52–58. https://doi.org/10.1038/nclimate1633
15. De Rossi, S., Di Marco, G., Bruno, L., Gismondi, A., Canini, A., 2021. Investigating the Drought and Salinity Effect on the Redox Components of Sulla Coronaria (L.) Medik. Antioxidants (Basel) 10, 1048. https://doi.org/10.3390/antiox10071048
16. Didaran, F., Kordrostami, M., Ghasemi-Soloklui, A.A., Pashkovskiy, P., Kreslavski, V., Kuznetsov, V., Allakhverdiev, S.I., 2024. The mechanisms of photoinhibition and repair in plants under high light conditions and interplay with abiotic stressors. Journal of Photochemistry and Photobiology B: Biology 259, 113004. https://doi.org/10.1016/j.jphotobiol.2024.113004
17. Dreyer, I., Hernández-Rojas, N., Bolua-Hernández, Y., Tapia-Castillo, V. de los A., Astola-Mariscal, S.Z., Díaz-Pico, E., Mérida-Quesada, F., Vergara-Valladares, F., Arrey-Salas, O., Rubio-Meléndez, M.E., Riedelsberger, J., Michard, E., 2024. Homeostats: The hidden rulers of ion homeostasis in plants. Quantitative Plant Biology 5, e8. https://doi.org/10.1017/qpb.2024.8
18. Dwivedi, S.L., Reynolds, M.P., Ortiz, R., 2021. Mitigating tradeoffs in plant breeding. iScience 24, 102965. https://doi.org/10.1016/j.isci.2021.102965
19. Eisenach, C., Chen, Z.-H., Grefen, C., Blatt, M.R., 2012. The trafficking protein SYP121 of Arabidopsis connects programmed stomatal closure and K+ channel activity with vegetative growth. The Plant Journal 69, 241–251. https://doi.org/10.1111/j.1365-313X.2011.04786.x
20. Emami Bistgani, Z., Barker, A.V., Hashemi, M., 2024. Physiology of medicinal and aromatic plants under drought stress. The Crop Journal 12, 330–339. https://doi.org/10.1016/j.cj.2023.12.003
21. Fahad, S., Bajwa, A.A., Nazir, U., Anjum, S.A., Farooq, A., Zohaib, A., Sadia, S., Nasim, W., Adkins, S., Saud, S., Ihsan, M.Z., Alharby, H., Wu, C., Wang, D., Huang, J., 2017. Crop Production under Drought and Heat Stress: Plant Responses and Management Options. Front. Plant Sci. 8. https://doi.org/10.3389/fpls.2017.01147

22. Gaccione, L., Martina, M., Barchi, L., Portis, E., 2023. A Compendium for Novel Marker-Based Breeding Strategies in Eggplant. Plants 12, 1016. https://doi.org/10.3390/plants12051016
23. Gaccione, L., Toppino, L., Bolger, M., Schmidt, M., Tassone, M.R., Sulli, M., Idahl, E., Alonso, D., Aprea, G., Ferrante, P., Lefebvre, V., Boyaci, H.F., Schafleitner, R., Gattolin, S., Finkers, R., Brouwer, M., Bovy, A., Prohens, J., Portis, E., Lanteri, S., Rotino, G.L., Giuliano, G., Usadel, B., Barchi, L., 2025. Graph-based pangenomes and pan-phenome provide a cornerstone for eggplant biology and breeding. Nat Commun 16, 9919. https://doi.org/10.1038/s41467-025-64866-1
24. Gao, Y., Li, X., Han, C., Huang, Q., Wu, R., Zhao, C., She, K., 2026. Photosystem vulnerabilities under compound abiotic stresses: mechanisms, diagnostics, and engineering for resilient crops. Plant Stress 19, 101193. https://doi.org/10.1016/j.stress.2025.101193
25. González-Orenga, S., Plazas, M., Ribera, E., Pallotti, C., Boscaiu, M., Prohens, J., Vicente, O., Fita, A., 2023. Transgressive Biochemical Response to Water Stress in Interspecific Eggplant Hybrids. Plants 12, 194. https://doi.org/10.3390/plants12010194
26. Haghpanah, M., Hashemipetroudi, S., Arzani, A., Araniti, F., 2024. Drought Tolerance in Plants: Physiological and Molecular Responses. Plants 13, 2962. https://doi.org/10.3390/plants13212962
27. Haile, G.G., Tang, Q., Reda, K.W., Baniya, B., He, L., Wang, Y., Gebrechorkos, S.H., 2024. Projected impacts of climate change on global irrigation water withdrawals. Agricultural Water Management 305, 109144. https://doi.org/10.1016/j.agwat.2024.109144
28. Han, D., Lu, J., Zhao, C., Ali, S., Jiang, Z., 2026. The Role and Regulatory Mechanisms of Cuticular Wax in Crop Stress Tolerance and Yield. Plants 15. https://doi.org/10.3390/plants15040554
29. Irshad, I.U., Sharma, A.K., 2024. Understanding the regulation of protein synthesis under stress conditions. Biophys J 123, 3627–3639. https://doi.org/10.1016/j.bpj.2024.09.014
30. Jiang, Z., van Zanten, M., Sasidharan, R., 2025. Mechanisms of plant acclimation to multiple abiotic stresses. Commun Biol 8, 655. https://doi.org/10.1038/s42003-025-08077-w
31. Jurado-Mañogil, C., Martínez-Melgarejo, P.A., Martínez-García, P., Rubio, M., Hernández, J.A., Barba-Espín, G., Diaz-Vivancos, P., Martínez-García, P.J., 2024. Comprehensive study of the hormonal, enzymatic and osmoregulatory response to drought in Prunus species. Scientia Horticulturae 326, 112786. https://doi.org/10.1016/j.scienta.2023.112786
32. Karami, S., Shiran, B., Ravash, R., 2025. Molecular investigation of how drought stress affects chlorophyll metabolism and photosynthesis in leaves of C3 and C4 plant species: A transcriptome meta-analysis. Heliyon 11, e42368. https://doi.org/10.1016/j.heliyon.2025.e42368
33. Khan, M.I.R., Kumari, S., Nazir, F., Khanna, R.R., Gupta, R., Chhillar, H., 2023. Defensive Role of Plant Hormones in Advancing Abiotic Stress-Resistant Rice Plants. Rice Science 30, 15–35. https://doi.org/10.1016/j.rsci.2022.08.002
34. Kolde, R., 2010. pheatmap: Pretty Heatmaps. https://doi.org/10.32614/CRAN.package.pheatmap
35. Langfelder, P., Horvath, S., 2008. WGCNA: an R package for weighted correlation network analysis. BMC Bioinformatics 9, 559. https://doi.org/10.1186/1471-2105-9-559
36. Leisner, C.P., Potnis, N., Sanz-Saez, A., 2023. Crosstalk and trade-offs: Plant responses to climate change-associated abiotic and biotic stresses. Plant, Cell & Environment 46, 2946–2963. https://doi.org/10.1111/pce.14532
37. Li, D., Gachie, S.W., Ozawa, S., Scholz, M., Hippler, M., Sakamoto, W., 2026. Chloroplast heat shock protein cpHsc70-1 interacts with thylakoid membrane

remodeling protein VIPP1 C-terminal tail and controls VIPP1 oligomer assembly. PNAS Nexus 5, pgaf393. https://doi.org/10.1093/pnasnexus/pgaf393
38. Li, S., Qiao, Z., Zhang, X., Zou, M., Hu, Y., Wei, D., Tang, Q., Yang, Y., Wang, Z., 2025. Transcription factor SmMYC2 regulates secondary cell wall thickening to enhance drought resilience in eggplant. Plant Cell Rep 44, 272. https://doi.org/10.1007/s00299-025-03657-w
39. Liao, Z., Zhang, Y., Yu, Q., Fang, W., Chen, M., Li, T., Liu, Y., Liu, Z., Chen, L., Yu, S., Xia, H., Xue, H.-W., Yu, H., Luo, L., 2023. Coordination of growth and drought responses by GA-ABA signaling in rice. New Phytologist 240, 1149–1161. https://doi.org/10.1111/nph.19209
40. Love, M.I., Huber, W., Anders, S., 2014. Moderated estimation of fold change and dispersion for RNA-seq data with DESeq2. Genome Biol 15, 550. https://doi.org/10.1186/s13059-014-0550-8
41. Lu, Y., Duursma, R.A., Farrior, C.E., Medlyn, B.E., Feng, X., 2020. Optimal stomatal drought response shaped by competition for water and hydraulic risk can explain plant trait covariation. New Phytologist 225, 1206–1217. https://doi.org/10.1111/nph.16207
42. Maioli, A., De Marchi, F., Valentino, D., Gianoglio, S., Patono, D.L., Miloro, F., Bai, Y., Comino, C., Lanteri, S., Lovisolo, C., Acquadro, A., Moglia, A., 2024. Knock-out of *SlDMR6-1* in tomato promotes a drought-avoidance strategy and increases tolerance to Late Blight. Plant Stress 13, 100541. https://doi.org/10.1016/j.stress.2024.100541
43. Martina, M., De Rosa, V., Magon, G., Acquadro, A., Barchi, L., Barcaccia, G., De Paoli, E., Vannozzi, A., Portis, E., 2024. Revitalizing agriculture: next-generation genotyping and -omics technologies enabling molecular prediction of resilient traits in the Solanaceae family. Frontiers in Plant Science 15.
44. Martins, J., Neves, M., Canhoto, J., 2023. Drought-Stress-Induced Changes in Chloroplast Gene Expression in Two Contrasting Strawberry Tree (Arbutus unedo L.) Genotypes. Plants 12. https://doi.org/10.3390/plants12244133
45. Morabito, C., Orozco, J., Tonel, G., Cavalletto, S., Meloni, G.R., Schubert, A., Gullino, M.L., Zwieniecki, M.A., Secchi, F., 2022. Do the ends justify the means? Impact of drought progression rate on stress response and recovery in Vitis vinifera. Physiol Plant 174, e13590. https://doi.org/10.1111/ppl.13590
46. Muhammad Aslam, M., Waseem, M., Jakada, B.H., Okal, E.J., Lei, Z., Saqib, H.S.A., Yuan, W., Xu, W., Zhang, Q., 2022. Mechanisms of Abscisic Acid-Mediated Drought Stress Responses in Plants. Int J Mol Sci 23, 1084. https://doi.org/10.3390/ijms23031084
47. Muñoz-Mayor, A., Pineda, B., Garcia-Abellán, J.O., Antón, T., Garcia-Sogo, B., Sanchez-Bel, P., Flores, F.B., Atarés, A., Angosto, T., Pintor-Toro, J.A., Moreno, V., Bolarin, M.C., 2012. Overexpression of dehydrin *tas14* gene improves the osmotic stress imposed by drought and salinity in tomato. Journal of Plant Physiology 169, 459–468. https://doi.org/10.1016/j.jplph.2011.11.018
48. Nagahatenna, D.S.K., Langridge, P., Whitford, R., 2015. Tetrapyrrole-based drought stress signalling. Plant Biotechnol J 13, 447–459. https://doi.org/10.1111/pbi.12356
49. Nour, M.M., Aljabi, H.R., AL-Huqail, A.A., Horneburg, B., Mohammed, A.E., Alotaibi, M.O., 2024. Drought responses and adaptation in plants differing in life-form. Front. Ecol. Evol. 12. https://doi.org/10.3389/fevo.2024.1452427
50. Ojeilua, C.H., Atijosan, O.E., Rahmon, M.A., Oyeyinka, B.O., Kaura, S., Chizoba, A.P., Onophurhi, G.A., 2025. Dual Drought–Lead Stress Tolerance in Solanaceae: Morphophysiological and Genetic Integration. African Journal of Agricultural Science and Food Research 20, 01–33. https://doi.org/10.62154/ajasfr.2025.020.01011
51. Paladini, F., Patono, D.L., De Palo, F., Acquadro, A., Lovisolo, C., 2025. Can high-throughput 3D and multispectral phenotyping detect early grapevine responses to water stress events? Plant Science 360, 112725. https://doi.org/10.1016/j.plantsci.2025.112725

52. Pang, X., Chen, J., Li, L., Huang, W., Liu, J., 2024. Deciphering Drought Resilience in Solanaceae Crops: Unraveling Molecular and Genetic Mechanisms. Biology (Basel) 13, 1076. https://doi.org/10.3390/biology13121076
53. Patro, R., Duggal, G., Love, M.I., Irizarry, R.A., Kingsford, C., 2017. Salmon: fast and bias-aware quantification of transcript expression using dual-phase inference. Nat Methods 14, 417–419. https://doi.org/10.1038/nmeth.4197
54. Qiao, M., Hong, C., Jiao, Y., Hou, S., Gao, H., 2024. Impacts of Drought on Photosynthesis in Major Food Crops and the Related Mechanisms of Plant Responses to Drought. Plants 13. https://doi.org/10.3390/plants13131808
55. Refaiy, A., Lilley, C.J., Atkinson, N.J., Urwin, P.E., 2026. Drought stress modulates the molecular response of Arabidopsis plants to root-knot nematode infection. Environmental and Experimental Botany 241, 106308. https://doi.org/10.1016/j.envexpbot.2025.106308
56. Saptiningsih, E., Darmanti, S., Setiari, N., 2023. Tolerance of Capsicum frutescens L. (Solanales: Solanaceae) to the duration of waterlogging and impact on the post-waterlogging and recovery periods. Natural History Sciences 10. https://doi.org/10.4081/nhs.2023.641
57. Sękara, A., Bączek-Kwinta, R., Gawęda, M., Kalisz, A., Pokluda, R., Jezdinský, A., 2016. Sequential abiotic stress applied to juvenile eggplant modifies the seedlings parameters, plant ontogeny and yield. Horticultural Science 43, 149–157. https://doi.org/10.17221/162/2015-HORTSCI
58. Seleiman, M.F., Al-Suhaibani, N., Ali, N., Akmal, M., Alotaibi, M., Refay, Y., Dindaroglu, T., Abdul-Wajid, H.H., Battaglia, M.L., 2021. Drought Stress Impacts on Plants and Different Approaches to Alleviate Its Adverse Effects. Plants (Basel) 10, 259. https://doi.org/10.3390/plants10020259
59. Skubacz, A., Daszkowska-Golec, A., Szarejko, I., 2016. The Role and Regulation of ABI5 (ABA-Insensitive 5) in Plant Development, Abiotic Stress Responses and Phytohormone Crosstalk. Front. Plant Sci. 7. https://doi.org/10.3389/fpls.2016.01884
60. Soma, F., Takahashi, F., Yamaguchi-Shinozaki, K., Shinozaki, K., 2021. Cellular Phosphorylation Signaling and Gene Expression in Drought Stress Responses: ABA-Dependent and ABA-Independent Regulatory Systems. Plants (Basel) 10, 756. https://doi.org/10.3390/plants10040756
61. Soneson, C., Love, M.I., Robinson, M.D., 2015. Differential analyses for RNA-seq: transcript-level estimates improve gene-level inferences. F1000Res 4, 1521. https://doi.org/10.12688/f1000research.7563.2
62. Suzuki, N., Koussevitzky, S., Mittler, R., Miller, G., 2012. ROS and redox signalling in the response of plants to abiotic stress. Plant, Cell & Environment 35, 259–270. https://doi.org/10.1111/j.1365-3040.2011.02336.x
63. Toppino, L., Barchi, L., Rotino, G.L., 2022. Next Generation Breeding for Abiotic Stress Resistance in Eggplant, in: Kole, C. (Ed.), Genomic Designing for Abiotic Stress Resistant Vegetable Crops. Springer International Publishing, Cham, pp. 115–151. https://doi.org/10.1007/978-3-031-03964-5_4
64. Vaseva, I.I., Balzhyk, H., Trailova, M., Nikolova, T., Katerova, Z., Galabova, S., Todorova, D., Sergiev, I., Vassileva, V., 2025. Ethylene Signaling Modulates Dehydrin Expression in Arabidopsis thaliana Under Prolonged Dehydration. Int J Mol Sci 26, 4148. https://doi.org/10.3390/ijms26094148
65. Villanueva, G., Mauceri, A., Misale, L., Abenavoli, M.R., Gramazio, P., Vilanova, S., Plazas, M., Prohens, J., Sunseri, F., 2026. Performance and QTL mapping of eggplant lines with *Solanum insanum* introgressions under contrasting nitrogen levels in substrate and hydroponic growing systems. Plant Stress 19, 101248. https://doi.org/10.1016/j.stress.2026.101248
66. Villanueva, G., Vilanova, S., Plazas, M., Prohens, J., Gramazio, P., 2023. Transcriptome profiles of eggplant (*Solanum melongena*) and its wild relative *S. dasyphyllum* under different levels of osmotic stress provide insights into response

mechanisms to drought. Current Plant Biology 33, 100276. https://doi.org/10.1016/j.cpb.2023.100276
67. Wadood, A., Hameed, A., Akram, S., Ghaffar, M., 2024. Unraveling the impact of water deficit stress on nutritional quality and defense response of tomato genotypes. Front. Plant Sci. 15. https://doi.org/10.3389/fpls.2024.1403895
68. Wang, M., Zhao, Y., Huang, Y., Liu, J., 2025. Integrating Drought Stress Signaling and Smart Breeding for Climate-Resilient Crops: Regulatory Mechanisms and Genetic Strategies. Plants 14. https://doi.org/10.3390/plants14243714
69. Wang, S., Ma, Q., Li, C., Zhang, S., Liu, X., 2025. Chloroplast Responses to Drought: Integrative Mechanisms and Mitigation Strategies. International Journal of Molecular Sciences 26. https://doi.org/10.3390/ijms262411872
70. Wei, Y., Liu, W., Hu, W., Yan, Y., Shi, H., 2020. The chaperone MeHSP90 recruits MeWRKY20 and MeCatalase1 to regulate drought stress resistance in cassava. New Phytologist 226, 476–491. https://doi.org/10.1111/nph.16346
71. Wei, Y.-S., Javed, T., Liu, T.-T., Ali, A., Gao, S.-J., 2025. Mechanisms of Abscisic acid (ABA)-mediated plant defense responses: An updated review. Plant Stress 15, 100724. https://doi.org/10.1016/j.stress.2024.100724
72. Yıldız, M.T., Akı, C., 2025. Evaluation of Physiological and Biochemical Responses of Four Tomato (Solanum lycopersicum L.) Cultivars at Different Drought Stress Levels. Agronomy 15. https://doi.org/10.3390/agronomy15030653
73. Yu, Z., Waheed, A., Zhang, D., Ismayil, A., Haxim, Y., 2025. Autophagy-Mediated Adaptation: Revealing the Role of Autophagy in Plant Responses to Abiotic Stress. Genes (Basel) 16, 1461. https://doi.org/10.3390/genes16121461
74. Zhao, P., Li, Qianqian, Lei, Y., Zou, J., Li, Qiang, 2025. Adaptation of cuticle metabolism to abiotic stress in plants. Crop and Environment 4, 38–44. https://doi.org/10.1016/j.crope.2025.01.001

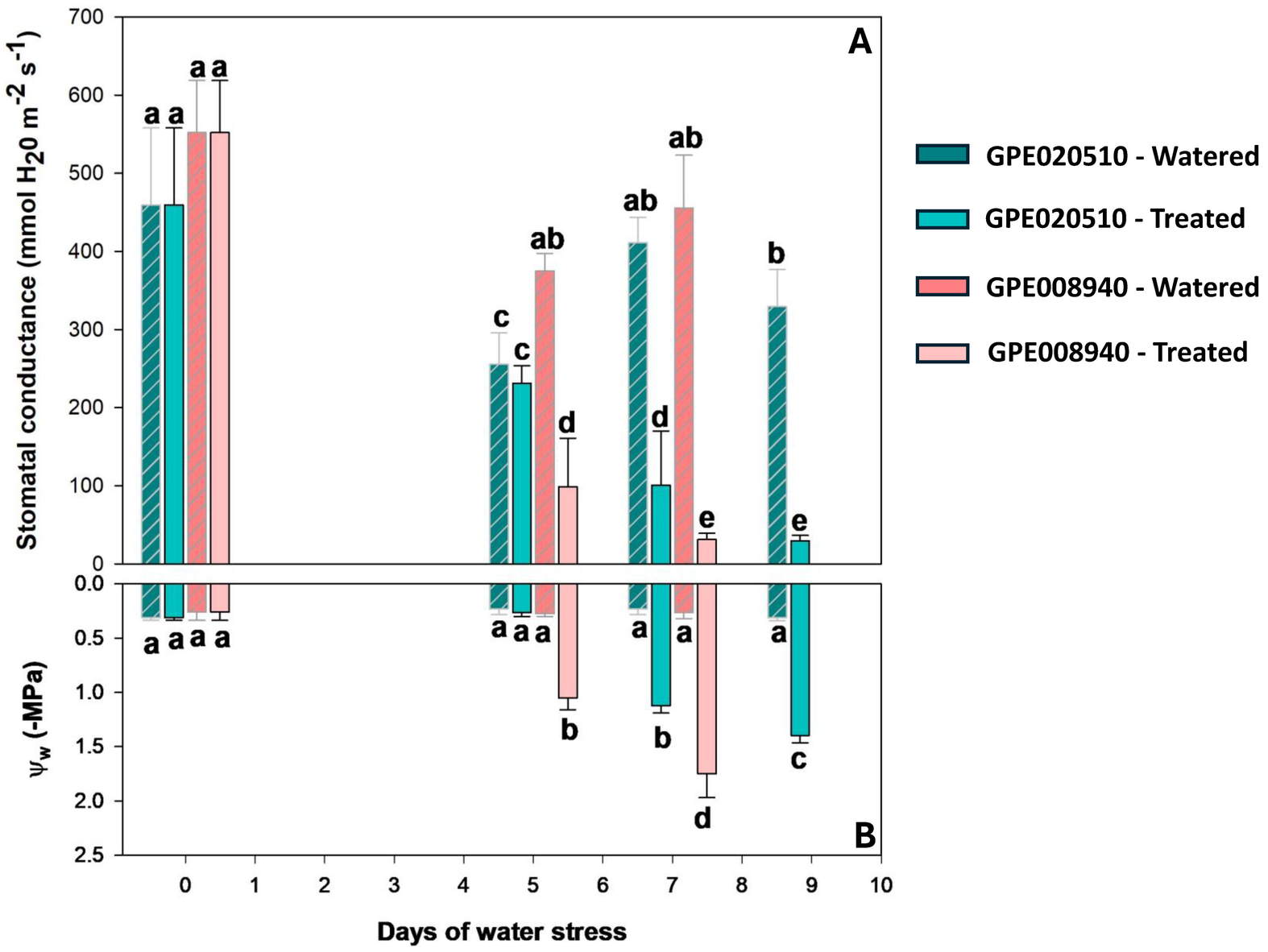
A
B
Stomatal conductance (mmol H20 m-2 s-1)
ψw (-MPa)
Days of water stress
GPE020510 - Watered
GPE020510 - Treated
GPE008940 - Watered
GPE008940 - Treated

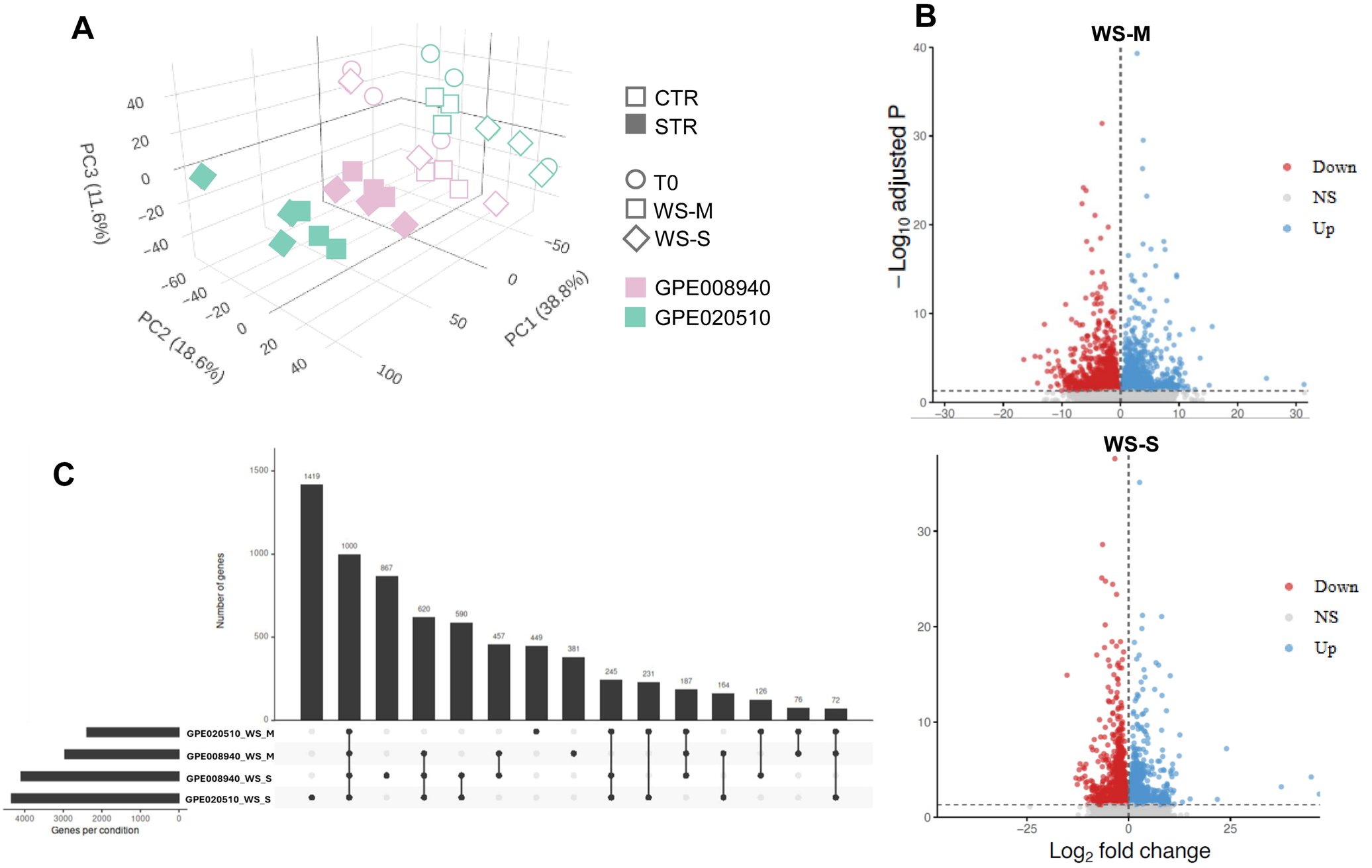
A
PC3 (11.6%)
PC2 (18.6%)
PC1 (38.8%)
CTR
STR
T0
WS-M
WS-S
GPE008940
GPE020510
B
WS-M
WS-S
$-\text{Log}_{10}$ adjusted P
Log_2 fold change
Down
NS
Up
C
Number of genes
Genes per condition
GPE020510_WS_M
GPE008940_WS_M
GPE008940_WS_S
GPE020510_WS_S
1419
1000
867
620
590
457
449
381
245
231
187
164
126
76
72

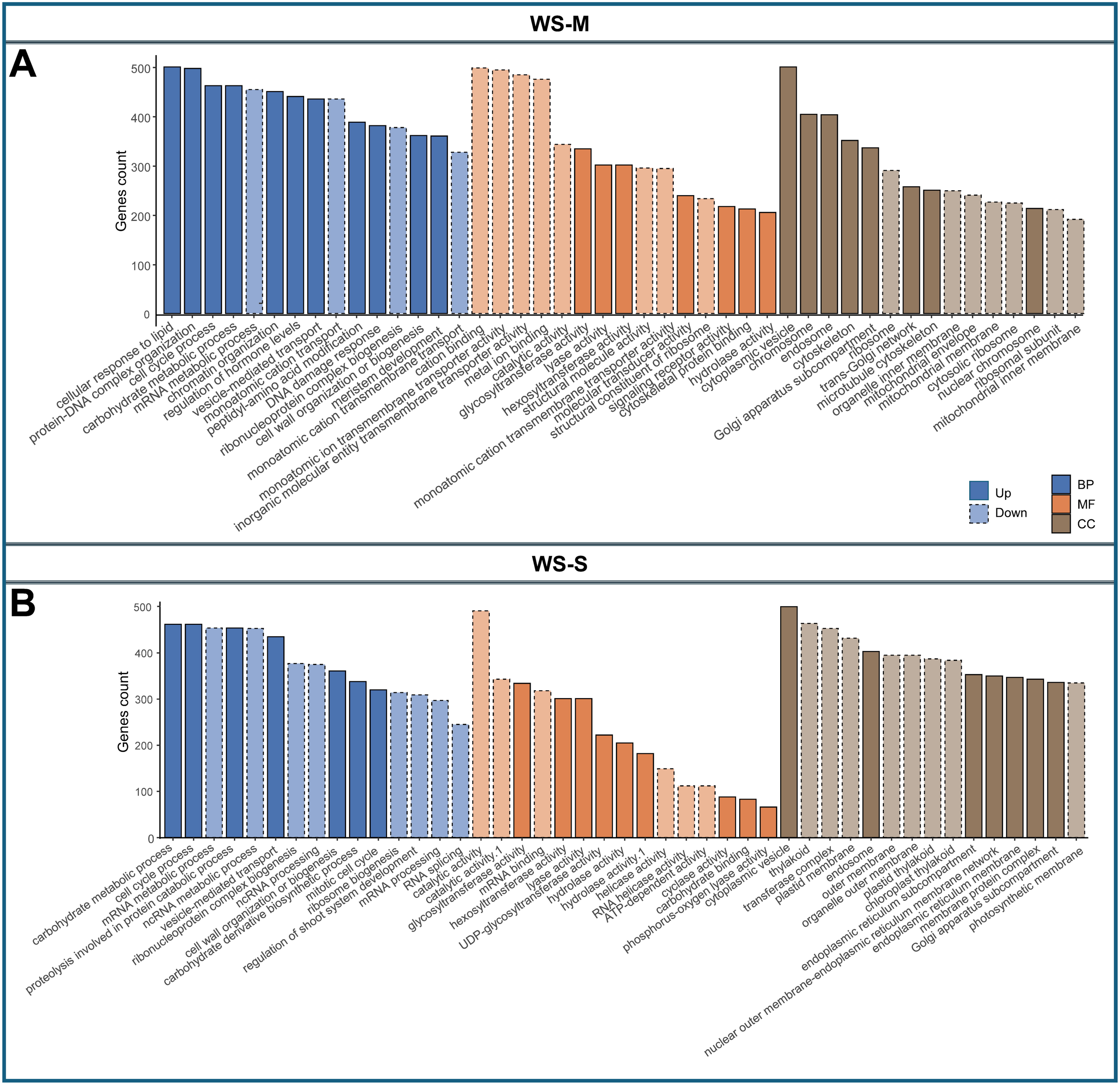
WS-M
A
Genes count
500
400
300
200
100
0
cellular response to lipid
protein-DNA complex organization
cell cycle process
carbohydrate metabolic process
mRNA metabolic process
chromatin organization
regulation of hormone levels
vesicle-mediated transport
monoatomic cation transport
peptidyl-amino acid modification
DNA damage response
ribonucleoprotein complex biogenesis
cell wall organization or biogenesis
meristem development
monoatomic cation transmembrane transport
cation binding
monoatomic ion transmembrane transporter activity
inorganic molecular entity transmembrane transporter activity
metal ion binding
catalytic activity
glycosyltransferase activity
lyase activity
hexosyltransferase activity
structural molecule activity
monoatomic cation transmembrane transporter activity
molecular transducer activity
structural constituent of ribosome
signaling receptor activity
cytoskeletal protein binding
hydrolase activity
cytoplasmic vesicle
chromosome
endosome
cytoskeleton
Golgi apparatus subcompartment
ribosome
trans-Golgi network
microtubule cytoskeleton
organelle inner membrane
mitochondrial envelope
mitochondrial membrane
cytosolic ribosome
nuclear chromosome
ribosomal subunit
mitochondrial inner membrane
Up
Down
BP
MF
CC
WS-S
B
Genes count
500
400
300
200
100
0
carbohydrate metabolic process
cell cycle process
mRNA metabolic process
proteolysis involved in protein catabolic process
ncRNA metabolic process
vesicle-mediated transport
ribonucleoprotein complex biogenesis
ncRNA processing
cell wall organization or biogenesis
carbohydrate derivative biosynthetic process
mitotic cell cycle
regulation of shoot system development
ribosome biogenesis
mRNA processing
RNA splicing
catalytic activity
catalytic activity.1
glycosyltransferase activity
mRNA binding
hexosyltransferase activity
lyase activity
UDP-glycosyltransferase activity
hydrolase activity
hydrolase activity.1
helicase activity
RNA helicase activity
ATP-dependent activity
cyclase activity
carbohydrate binding
phosphorus-oxygen lyase activity
cytoplasmic vesicle
thylakoid
transferase complex
plastid membrane
endosome
outer membrane
organelle outer membrane
plastid thylakoid
chloroplast thylakoid
endoplasmic reticulum subcompartment
nuclear outer membrane-endoplasmic reticulum membrane network
endoplasmic reticulum membrane
membrane protein complex
Golgi apparatus subcompartment
photosynthetic membrane

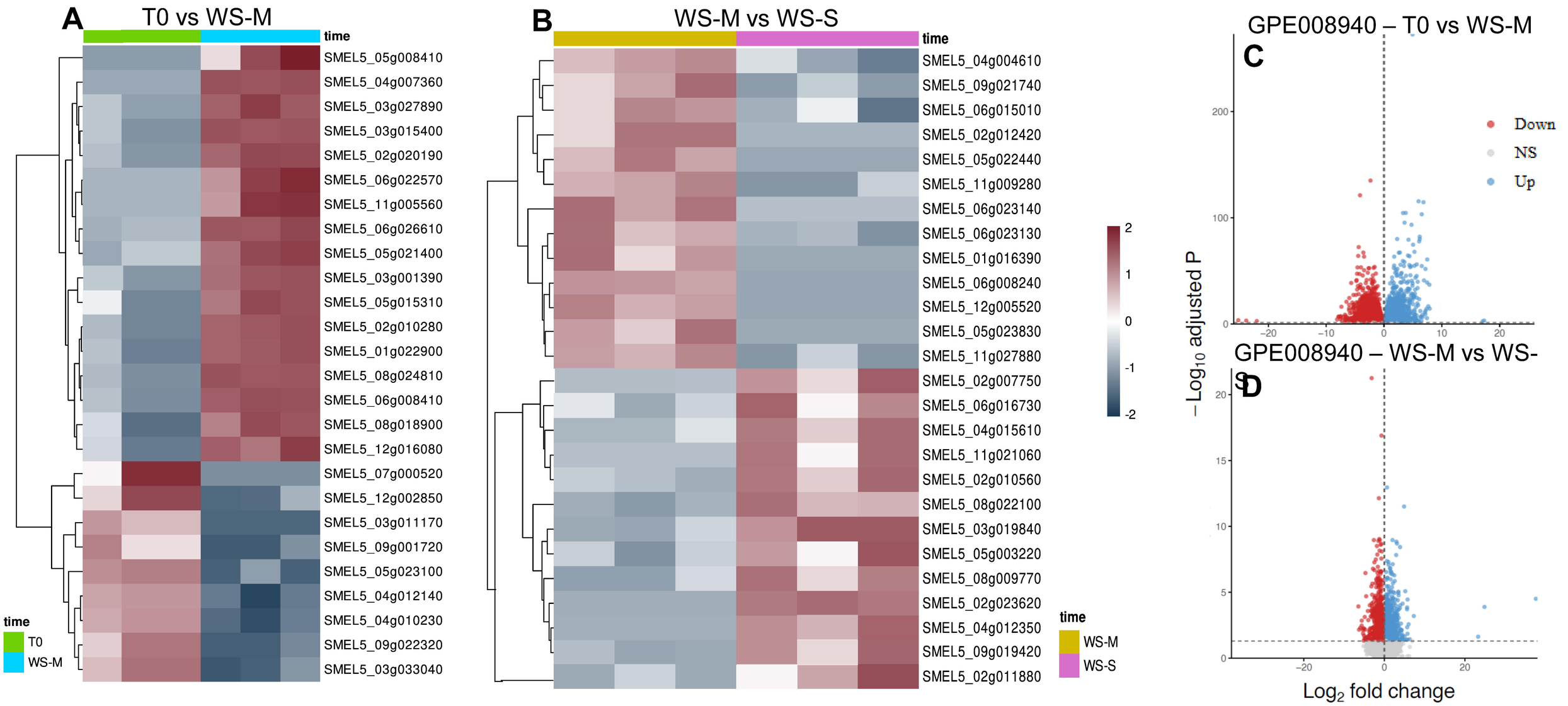
A
T0 vs WS-M
time
SMEL5_05g008410
SMEL5_04g007360
SMEL5_03g027890
SMEL5_03g015400
SMEL5_02g020190
SMEL5_06g022570
SMEL5_11g005560
SMEL5_06g026610
SMEL5_05g021400
SMEL5_03g001390
SMEL5_05g015310
SMEL5_02g010280
SMEL5_01g022900
SMEL5_08g024810
SMEL5_06g008410
SMEL5_08g018900
SMEL5_12g016080
SMEL5_07g000520
SMEL5_12g002850
SMEL5_03g011170
SMEL5_09g001720
SMEL5_05g023100
SMEL5_04g012140
SMEL5_04g010230
SMEL5_09g022320
SMEL5_03g033040
time
T0
WS-M
B
WS-M vs WS-S
time
SMEL5_04g004610
SMEL5_09g021740
SMEL5_06g015010
SMEL5_02g012420
SMEL5_05g022440
SMEL5_11g009280
SMEL5_06g023140
SMEL5_06g023130
SMEL5_01g016390
SMEL5_06g008240
SMEL5_12g005520
SMEL5_05g023830
SMEL5_11g027880
SMEL5_02g007750
SMEL5_06g016730
SMEL5_04g015610
SMEL5_11g021060
SMEL5_02g010560
SMEL5_08g022100
SMEL5_03g019840
SMEL5_05g003220
SMEL5_08g009770
SMEL5_02g023620
SMEL5_04g012350
SMEL5_09g019420
SMEL5_02g011880
2
1
0
-1
-2
time
WS-M
WS-S
GPE008940 – T0 vs WS-M
C
Down
NS
Up
200
100
0
−20
−10
0
10
20
GPE008940 – WS-M vs WS-S
D
20
15
10
5
0
−20
0
20
−Log10 adjusted P
Log2 fold change

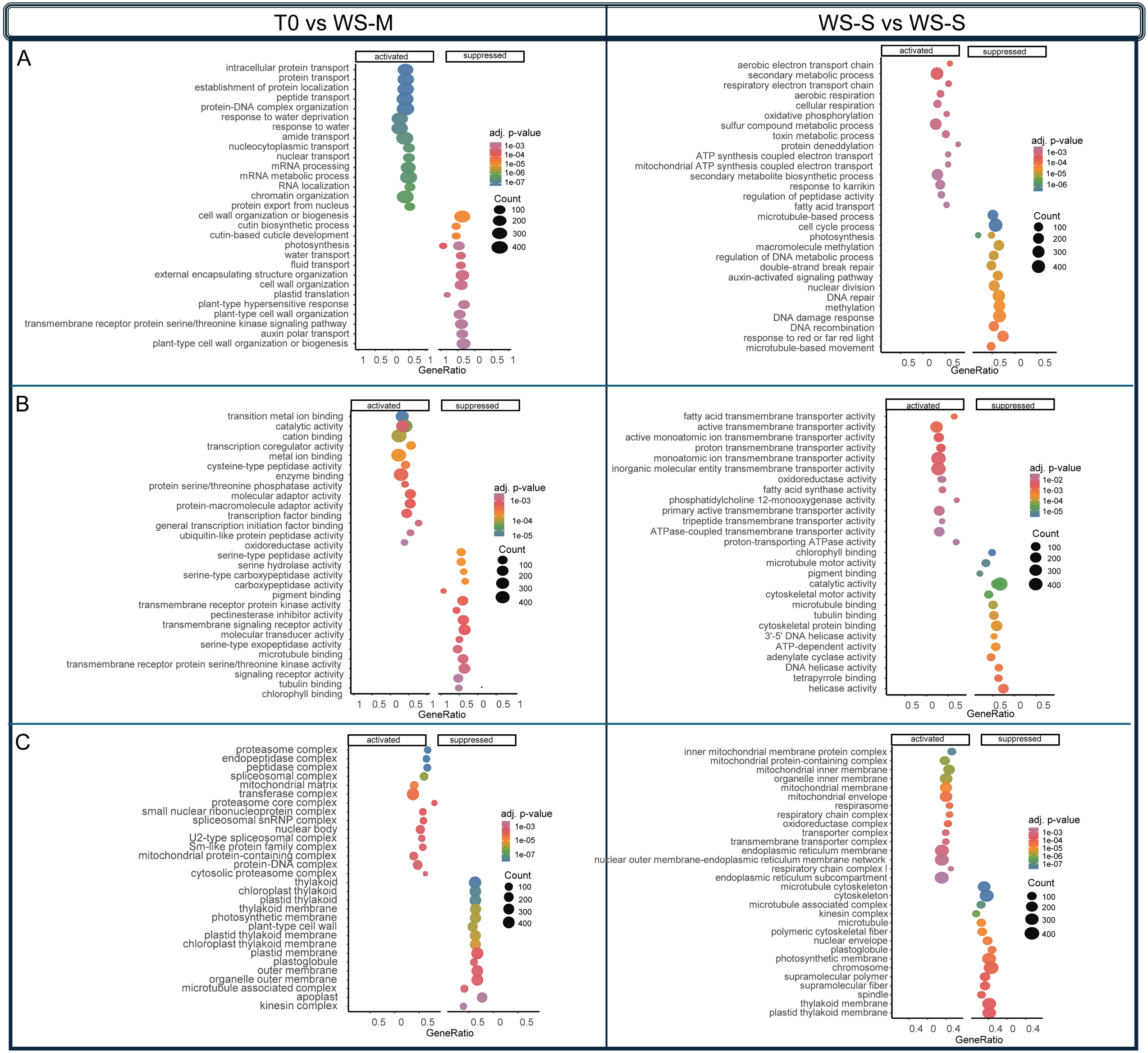
T0 vs WS-M
WS-S vs WS-S
A
activated
suppressed
intracellular protein transport
protein transport
establishment of protein localization
peptide transport
protein-DNA complex organization
response to water deprivation
response to water
amide transport
nucleocytoplasmic transport
nuclear transport
mRNA processing
mRNA metabolic process
RNA localization
chromatin organization
protein export from nucleus
cell wall organization or biogenesis
cutin biosynthetic process
cutin-based cuticle development
photosynthesis
water transport
fluid transport
external encapsulating structure organization
cell wall organization
plastid translation
plant-type hypersensitive response
plant-type cell wall organization
transmembrane receptor protein serine/threonine kinase signaling pathway
auxin polar transport
plant-type cell wall organization or biogenesis
adj. p-value
1e-03
1e-04
1e-05
1e-06
1e-07
Count
100
200
300
400
1 0.5 0 0.5 1 1 0.5 0 0.5 1
GeneRatio
aerobic electron transport chain
secondary metabolic process
respiratory electron transport chain
aerobic respiration
cellular respiration
oxidative phosphorylation
sulfur compound metabolic process
toxin metabolic process
protein deneddylation
ATP synthesis coupled electron transport
mitochondrial ATP synthesis coupled electron transport
secondary metabolite biosynthetic process
response to karrikin
regulation of peptidase activity
fatty acid transport
microtubule-based process
cell cycle process
photosynthesis
macromolecule methylation
regulation of DNA metabolic process
double-strand break repair
auxin-activated signaling pathway
nuclear division
DNA repair
methylation
DNA damage response
DNA recombination
response to red or far red light
microtubule-based movement
adj. p-value
1e-03
1e-04
1e-05
1e-06
Count
100
200
300
400
0.5 0 0.5 0.5 0 0.5
GeneRatio
B
activated
suppressed
transition metal ion binding
catalytic activity
cation binding
transcription coregulator activity
metal ion binding
cysteine-type peptidase activity
enzyme binding
protein serine/threonine phosphatase activity
molecular adaptor activity
protein-macromolecule adaptor activity
transcription factor binding
general transcription initiation factor binding
ubiquitin-like protein peptidase activity
oxidoreductase activity
serine-type peptidase activity
serine hydrolase activity
serine-type carboxypeptidase activity
carboxypeptidase activity
pigment binding
transmembrane receptor protein kinase activity
pectinesterase inhibitor activity
transmembrane signaling receptor activity
molecular transducer activity
serine-type exopeptidase activity
microtubule binding
transmembrane receptor protein serine/threonine kinase activity
signaling receptor activity
tubulin binding
chlorophyll binding
adj. p-value
1e-03
1e-04
1e-05
Count
100
200
300
400
1 0.5 0 0.5 1 1 0.5 0 0.5 1
GeneRatio
fatty acid transmembrane transporter activity
active transmembrane transporter activity
active monoatomic ion transmembrane transporter activity
proton transmembrane transporter activity
monoatomic ion transmembrane transporter activity
inorganic molecular entity transmembrane transporter activity
oxidoreductase activity
fatty acid synthase activity
phosphatidylcholine 12-monooxygenase activity
primary active transmembrane transporter activity
tripeptide transmembrane transporter activity
ATPase-coupled transmembrane transporter activity
proton-transporting ATPase activity
chlorophyll binding
microtubule motor activity
pigment binding
catalytic activity
cytoskeletal motor activity
microtubule binding
tubulin binding
cytoskeletal protein binding
3'-5' DNA helicase activity
ATP-dependent activity
adenylate cyclase activity
DNA helicase activity
tetrapyrrole binding
helicase activity
adj. p-value
1e-02
1e-03
1e-04
1e-05
Count
100
200
300
400
0.5 0 0.5 0.5 0 0.5
GeneRatio
C
activated
suppressed
proteasome complex
endopeptidase complex
peptidase complex
spliceosomal complex
mitochondrial matrix
transferase complex
proteasome core complex
small nuclear ribonucleoprotein complex
spliceosomal snRNP complex
nuclear body
U2-type spliceosomal complex
Sm-like protein family complex
mitochondrial protein-containing complex
protein-DNA complex
cytosolic proteasome complex
thylakoid
chloroplast thylakoid
plastid thylakoid
thylakoid membrane
photosynthetic membrane
plant-type cell wall
plastid thylakoid membrane
chloroplast thylakoid membrane
plastid membrane
plastoglobule
outer membrane
organelle outer membrane
microtubule associated complex
apoplast
kinesin complex
adj. p-value
1e-03
1e-05
1e-07
Count
100
200
300
400
0.5 0 0.5 0.5 0 0.5
GeneRatio
inner mitochondrial membrane protein complex
mitochondrial protein-containing complex
mitochondrial inner membrane
organelle inner membrane
mitochondrial membrane
mitochondrial envelope
respirasome
respiratory chain complex
oxidoreductase complex
transporter complex
transmembrane transporter complex
endoplasmic reticulum membrane
nuclear outer membrane-endoplasmic reticulum membrane network
respiratory chain complex I
endoplasmic reticulum subcompartment
microtubule cytoskeleton
cytoskeleton
microtubule associated complex
kinesin complex
microtubule
polymeric cytoskeletal fiber
nuclear envelope
plastoglobule
photosynthetic membrane
chromosome
supramolecular polymer
supramolecular fiber
spindle
thylakoid membrane
plastid thylakoid membrane
adj. p-value
1e-03
1e-04
1e-05
1e-06
1e-07
Count
100
200
300
400
0.4 0 0.4 0.4 0 0.4
GeneRatio

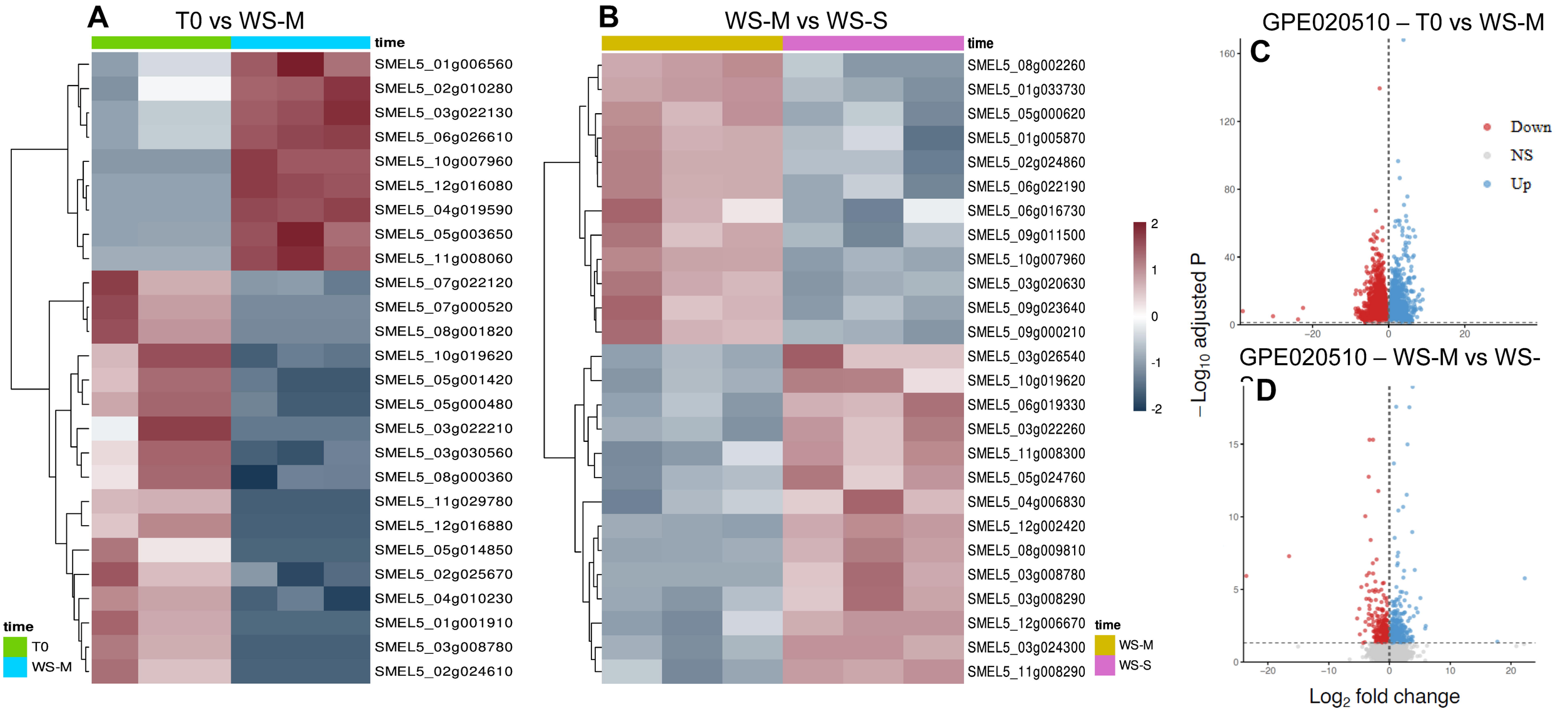
A
T0 vs WS-M
time
SMEL5_01g006560
SMEL5_02g010280
SMEL5_03g022130
SMEL5_06g026610
SMEL5_10g007960
SMEL5_12g016080
SMEL5_04g019590
SMEL5_05g003650
SMEL5_11g008060
SMEL5_07g022120
SMEL5_07g000520
SMEL5_08g001820
SMEL5_10g019620
SMEL5_05g001420
SMEL5_05g000480
SMEL5_03g022210
SMEL5_03g030560
SMEL5_08g000360
SMEL5_11g029780
SMEL5_12g016880
SMEL5_05g014850
SMEL5_02g025670
SMEL5_04g010230
SMEL5_01g001910
SMEL5_03g008780
SMEL5_02g024610
time
T0
WS-M
B
WS-M vs WS-S
time
SMEL5_08g002260
SMEL5_01g033730
SMEL5_05g000620
SMEL5_01g005870
SMEL5_02g024860
SMEL5_06g022190
SMEL5_06g016730
SMEL5_09g011500
SMEL5_10g007960
SMEL5_03g020630
SMEL5_09g023640
SMEL5_09g000210
SMEL5_03g026540
SMEL5_10g019620
SMEL5_06g019330
SMEL5_03g022260
SMEL5_11g008300
SMEL5_05g024760
SMEL5_04g006830
SMEL5_12g002420
SMEL5_08g009810
SMEL5_03g008780
SMEL5_03g008290
SMEL5_12g006670
SMEL5_03g024300
SMEL5_11g008290
2
1
0
-1
-2
time
WS-M
WS-S
GPE020510 – T0 vs WS-M
C
Down
NS
Up
GPE020510 – WS-M vs WS-S
D
– Log10 adjusted P
Log2 fold change

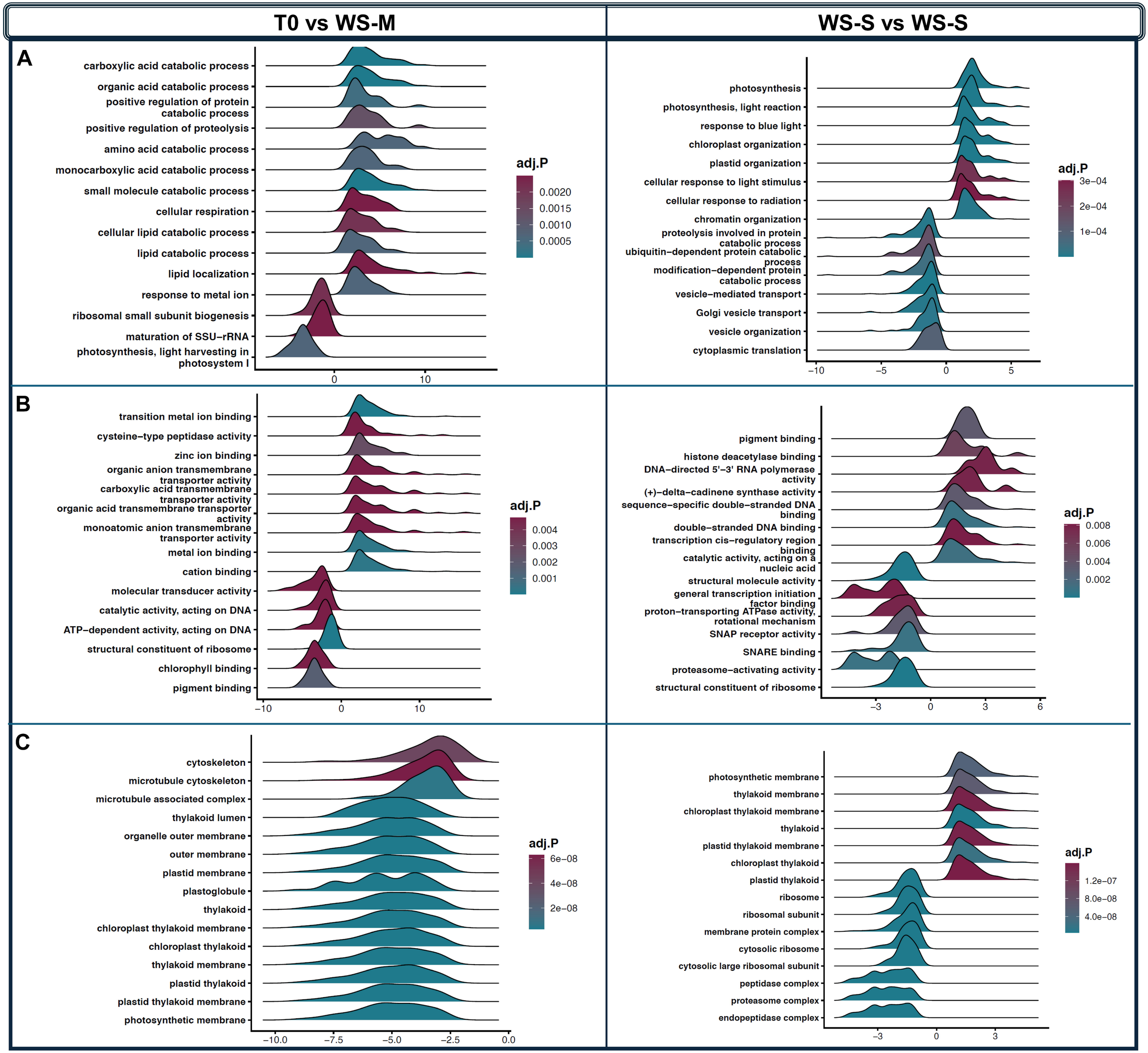
T0 vs WS-M
WS-S vs WS-S
A
carboxylic acid catabolic process
organic acid catabolic process
positive regulation of protein catabolic process
positive regulation of proteolysis
amino acid catabolic process
monocarboxylic acid catabolic process
small molecule catabolic process
cellular respiration
cellular lipid catabolic process
lipid catabolic process
lipid localization
response to metal ion
ribosomal small subunit biogenesis
maturation of SSU−rRNA
photosynthesis, light harvesting in photosystem I
0
10
adj.P
0.0020
0.0015
0.0010
0.0005
photosynthesis
photosynthesis, light reaction
response to blue light
chloroplast organization
plastid organization
cellular response to light stimulus
cellular response to radiation
chromatin organization
proteolysis involved in protein catabolic process
ubiquitin−dependent protein catabolic process
modification−dependent protein catabolic process
vesicle−mediated transport
Golgi vesicle transport
vesicle organization
cytoplasmic translation
−10
−5
0
5
adj.P
3e−04
2e−04
1e−04
B
transition metal ion binding
cysteine−type peptidase activity
zinc ion binding
organic anion transmembrane transporter activity
carboxylic acid transmembrane transporter activity
organic acid transmembrane transporter activity
monoatomic anion transmembrane transporter activity
metal ion binding
cation binding
molecular transducer activity
catalytic activity, acting on DNA
ATP−dependent activity, acting on DNA
structural constituent of ribosome
chlorophyll binding
pigment binding
−10
0
10
adj.P
0.004
0.003
0.002
0.001
pigment binding
histone deacetylase binding
DNA−directed 5'−3' RNA polymerase activity
(+)−delta−cadinene synthase activity
sequence−specific double−stranded DNA binding
double−stranded DNA binding
transcription cis−regulatory region binding
catalytic activity, acting on a nucleic acid
structural molecule activity
general transcription initiation factor binding
proton−transporting ATPase activity, rotational mechanism
SNAP receptor activity
SNARE binding
proteasome−activating activity
structural constituent of ribosome
−3
0
3
6
adj.P
0.008
0.006
0.004
0.002
C
cytoskeleton
microtubule cytoskeleton
microtubule associated complex
thylakoid lumen
organelle outer membrane
outer membrane
plastid membrane
plastoglobule
thylakoid
chloroplast thylakoid membrane
chloroplast thylakoid
thylakoid membrane
plastid thylakoid
plastid thylakoid membrane
photosynthetic membrane
−10.0
−7.5
−5.0
−2.5
0.0
adj.P
6e−08
4e−08
2e−08
photosynthetic membrane
thylakoid membrane
chloroplast thylakoid membrane
thylakoid
plastid thylakoid membrane
chloroplast thylakoid
plastid thylakoid
ribosome
ribosomal subunit
membrane protein complex
cytosolic ribosome
cytosolic large ribosomal subunit
peptidase complex
proteasome complex
endopeptidase complex
−3
0
3
adj.P
1.2e−07
8.0e−08
4.0e−08

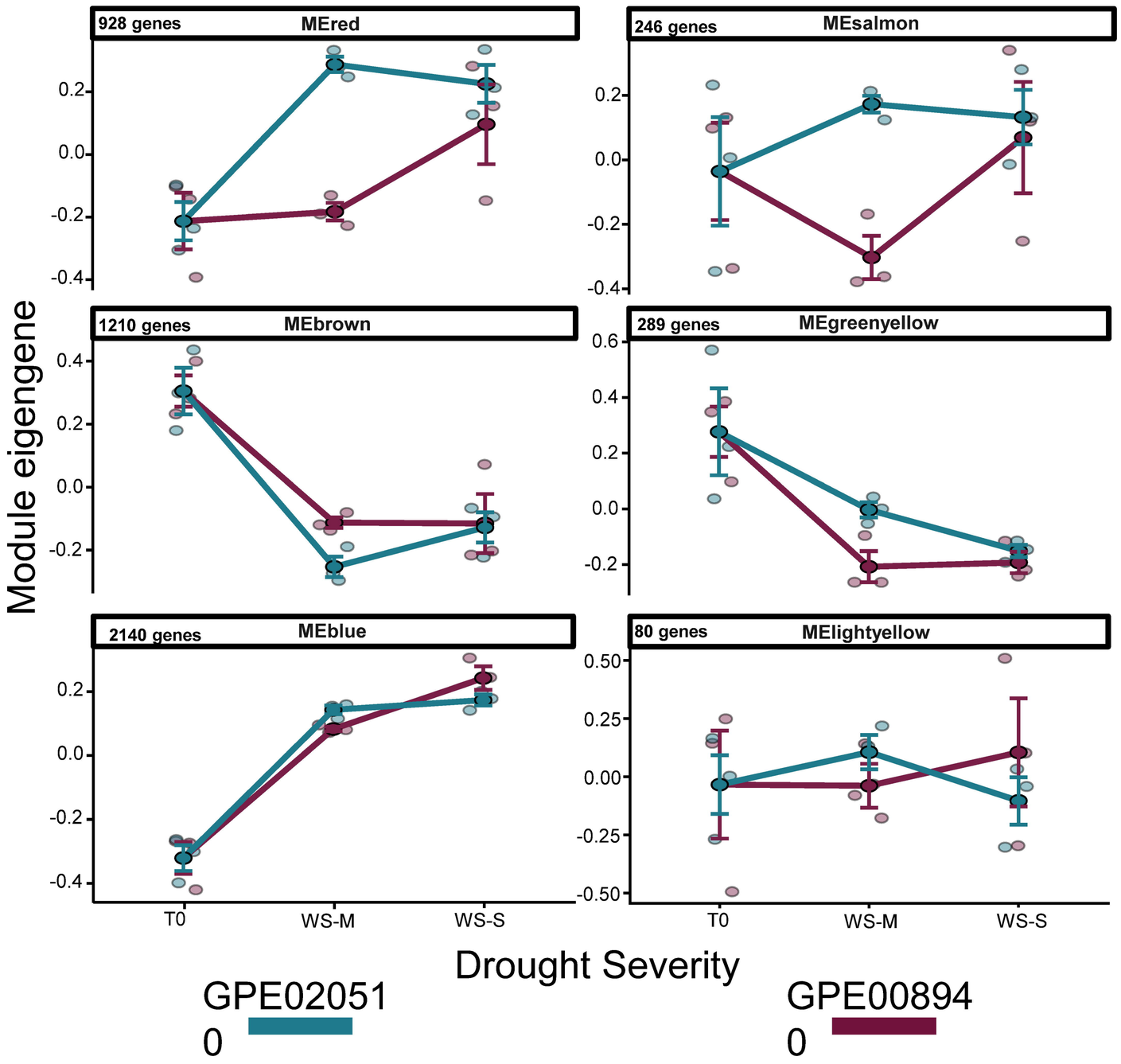
928 genes
MEred
246 genes
MEsalmon
1210 genes
MEbrown
289 genes
MEgreenyellow
2140 genes
MEblue
80 genes
MElightyellow
Module eigengene
T0
WS-M
WS-S
Drought Severity
GPE020510
GPE008940